Systems/Circuits

Specific Functional Connectivity of Molecular Subtypes of Subplate and Layer 6b Neurons

Minzi Chang,[1]* Zheng Xu,[1]* Sophia Nehs,[1] Yunru Chen,[1] Joseph P. Y. Kao,[2] and Patrick O. Kanold[1,3]

[1]Department of Biomedical Engineering, School of Medicine Johns Hopkins University, Baltimore, Maryland 21205, [2]Center for Biomedical Engineering and Technology, and Department of Physiology, University of Maryland School of Medicine, Baltimore, Maryland 21201, and [3]Kavli Neuroscience Discovery Institute, Johns Hopkins University, Baltimore, Maryland 21205

Subplate neurons (SpNs) are among the earliest generated cortical neurons that form functional cortical synapses and aid in cortical circuit development. A fraction of SpNs survive and form Layer (L)6b in the adult cortex. While SpNs exhibit a large variety of molecular identities, it is unclear if molecular identity correlates with their functional circuits and if different SpNs have similar developmental trajectories. To resolve these questions, we here characterize the functional intracortical circuits to molecularly identified subpopulations of SpNs with SpN-specific Cre-lines [connective tissue growth factor (CTGF)-dgCre and dopamine receptor D1 (Drd1)-Cre] in in vitro brain slices of the primary auditory cortex using whole-cell patch–clamp recordings and laser-scanning photostimulation. We targeted three age groups: before [Postnatal Day (P)7–P9] and after (P14–P20) the ear canal opening and when circuits are mature (P60–P80). While the excitatory intracortical circuits impinging on both subtypes were similar, inhibitory circuits differed, particularly those from subplate/L6b. At P7–P9, Drd1 neurons received stronger inhibition from the subplate compared with CTGF neurons. The functional circuits on SpNs prune with age. By P60–P80, the inhibitory connections from L6b on CTGF neurons increased and became significantly abundant than those on Drd1 neurons. However, the inhibition strength between the two subtypes remained unchanged. Thus, SpNs exhibit diverse neuronal morphologies and intracortical input patterns, independent of molecular expression. Thus, although the subplate comprises distinct molecular neural classes, molecular expression is not clearly correlated with neural morphologies and functional circuits throughout development.

Key words: **auditory cortex; circuits; development; mouse; slice; subplate**

Significance Statement

Subplate neurons (SpNs) pioneer cortical circuit formation and shape its maturation. SpNs can be categorized into different subpopulation based on their molecular identities. However, the relationship between functional circuitry and molecular identities was unclear. Our study demonstrated that excitatory inputs on different molecular classes of SpNs develop similarly but not the inhibitory inputs, particularly those from within subplate/Layer 6b. Moreover, SpNs within the same molecular classes exhibit diverse patterns of intracortical circuit connections and neuronal morphologies. This diversity becomes more pronounced in adulthood. Therefore, distinguishing the functional connectivity between the two subtypes based solely on their molecular identities is impossible. Overall, the molecular expression of SpNs is not clearly correlated with their morphologies and functional connectivity pattern.

Introduction

Proper sculpting of cortical circuits during development is crucial for normal wiring in the mature brain. One of the earliest generated populations in the cortical circuit are the subplate neurons (SpNs; Kostovic and Rakic, 1980; Luskin and Shatz, 1985; Valverde et al., 1989). SpNs are the first cortical neurons processing thalamic inputs (Friauf and Shatz, 1991; Higashi et al., 2002; Zhao et al., 2009; Wess et al., 2017; Molnár et al., 2020), and they are actively interconnected with cortical circuits during the early postnatal period (Viswanathan et al., 2012; Meng et al., 2014). As the brain matures, many SpNs undergo apoptosis, but the fraction of SpNs remaining in adults varies between species (Kanold and Luhmann, 2010; Chang and Kanold, 2021). In rodents, the reduction of the number of SpNs is small (Valverde et al., 1995; Price et al., 1997; Robertson et al., 2000), with most SpNs surviving to adulthood, forming Layer (L)6b (Clancy et al., 2001; Hoerder-Suabedissen et al., 2018). Early sensory experience can sculpt the morphology of

Received Nov. 5, 2024; revised Feb. 26, 2025; accepted March 2, 2025.

Author contributions: M.C. and P.O.K. designed research; M.C., Z.X., S.N., and Y.C. performed research; J.P.Y.K. contributed unpublished reagents/analytic tools; M.C., Z.X., and S.N. analyzed data; M.C. and P.O.K. wrote the paper.

This study was supported by NIH R01DC009607 (P.O.K.) and NIH R01GM056481 (J.P.Y.K.).

*M.C. and Z.X. contributed equally to this work.

The authors declare no competing financial interests.

Correspondence should be addressed to Patrick O. Kanold at pkanold@jhu.edu.

https://doi.org/10.1523/JNEUROSCI.2094-24.2025

Copyright © 2025 the authors

SpNs (Piñon et al., 2009) and the functional circuits on SpNs (Meng et al., 2021; Mukherjee et al., 2022, 2023), as well as L6b neurons (Yoneda et al., 2023). SpNs are involved in the patterning and functional maturation of thalamocortical connections (Ghosh and Shatz, 1993; Kanold et al., 2003; Tolner et al., 2012), critical period plasticity (Kanold and Shatz, 2006), and oligodendrocyte maturation (Yu et al., 2019). However, it is still unclear whether the general population of SpNs contributes to these biological processes or only a subpopulation of SpNs.

SpNs form subgroups based on molecular markers, connectivity patterns, and morphological properties (Hanganu et al., 2002; Hoerder-Suabedissen et al., 2009; Viswanathan et al., 2012; Hoerder-Suabedissen and Molnár, 2013; Meng et al., 2014; Marx et al., 2017). Molecular markers such as connective tissue growth factor (CTGF) and dopamine receptor D1 (Drd1) are expressed in SpNs (Hoerder-Suabedissen and Molnár, 2013; Hoerder-Suabedissen et al., 2018; Chang et al., 2024). The complement of SpN subpopulations differs between sensory cortices; for example, the developing auditory cortex (ACtx) contains more CTGF- than Drd1-expressing SpNs (Chang et al., 2024). While the Drd1 expression is not limited to subplate/L6b of the somatosensory and visual cortices (Hoerder-Suabedissen et al., 2018; Chang et al., 2024; Kim et al., 2024), their expression is confined to the ACtx subplate during the first three postnatal weeks (Chang et al., 2024). This provides a tool to explore how SpNs (or L6b neurons) subtypes are integrated into local circuits in the ACtx. While SpNs in the ACtx show changing and diverse cortical circuit patterns during the first two postnatal weeks (Viswanathan et al., 2012; Meng et al., 2014), the relationship between these patterns and molecular identities remains unclear. In addition, a prior study demonstrated that one-third of Drd1-expressing neurons in the somatosensory cortex are immunopositive for CTGF (Hoerder-Suabedissen et al., 2018). However, the proportion of this overlap in the ACtx remains unclear. We hypothesize that if a similar overlap exists in the ACtx, the distinct subpopulations of molecularly defined neurons (i.e., CTGF+, Drd1a+, CTGF+/Drd1a+) may exhibit unique intracortical circuit patterns, which could help explain the diversity of cortical circuit patterns observed in the ACtx during the first two postnatal weeks. As the brain matures, the remnants of SpNs, L6b neurons in the somatosensory cortex, also express CTGF and Drd1 and are thought to share similar functional, mainly long-range, cortical connectivity (Hoerder-Suabedissen et al., 2018; Zolnik et al., 2020). Functional changes in these circuits over age could be due to selective changes in the makeup of the subpopulation or functional changes for each molecularly defined subpopulation.

To address these issues, we determined (1) if molecularly defined SpNs share distinct cortical connectivity patterns and neuronal morphology and (2) whether their functional connections change similarly as the brain matures into adulthood. We address these questions by functionally characterizing intracortical circuits in molecularly identified subpopulations of SpNs in the primary ACtx (A1) of mice using laser-scanning photostimulation (LSPS). We used two subplate and L6b, specific mouse lines (Drd1-Cre and CTGF-Cre) within three age groups, P7–P9, P14–P20, and P60–P80, coinciding with the period before and after the ear canal opening, and when the cortical circuit is mature. Since, in visual and somatosensory cortices Drd1-positive neurons are also found outside L6b (Kim et al., 2024), we here restrict our analysis to neurons located within subplate/L6b based on their anatomical location in the ACtx. Our study demonstrated that the intrinsic properties of SpNs develop similarly, regardless of their molecular identities. However, during the early postnatal period, CTGF and Drd1 SpNs exhibit different circuitry patterns, especially inhibitory connections on these SpNs. Additionally, we found that even among the same molecularly defined SpN class, a large variety of connectivity patterns are present throughout development into adulthood. Thus, molecular subclasses of SpNs contain multiple functional subclasses, likely playing different roles during development and adulthood. Moreover, the molecular expression of SpNs is not correlated with their somatodendritic morphologies and functional intracortical connectivity patterns.

Materials and Methods

Animals. All experiments and procedures were approved by the Johns Hopkins Institutional Care and Use Committee. Animals were provided with food and water *ad libitum* and maintained on a regular 12 h day/night cycle. Mice that are heterozygous for Drd1-Cre [*Tg(Drd1-cre)FK164Gsat/Mmucd*, MMRRC Stock 030781-UCD] or CTGF-Cre (*CTGF-2A-dgCre*, JAX stock #028535) were bred with homozygous tdTomato floxed reporter mice [*Gt(ROSA)26Sor*$^{tm9(CAG\text{-}tdTomato)Hze}$*/J*, JAX stock #007909]. The offspring were genotyped by TransnetYX, and only those that were heterozygous for Cre recombinase and expressing tdTomato reporter (i.e., CTGF$^{Cre/+}$;tdTomato$^{fl/+}$ or Drd1$^{Cre/+}$;tdTomato$^{fl/+}$) were used in this experiment. CTGF is transiently expressed in the vasculature from Embryonic Day (E)18 to Postnatal Day (P)3 (Friedrichsen et al., 2003). To suppress CTGF expression in the blood vessels, we stabilize the Cre expression in CTGF-Cre mice by administering 150 µg/g of trimethoprim (Sigma-Aldrich, T0667) into the milk sac of animals at P4 and P5. Cre induction was not necessary for Drd1-Cre animals. Both sexes of the mice were harvested at three different time windows: (1) P7–P9, (2) P14–P20, and (3) P60–P80 (Fig. 1*A*).

Preparation of auditory thalamocortical slices. In vitro slice recordings from SpNs in A1 were performed as previously described (Cruikshank et al., 2002; Zhao et al., 2009; Meng et al., 2014). Briefly, mice were deeply anesthetized with isoflurane before decapitation. The brain was quickly transferred to ice-cold dissecting solution (in mM), 212.7 sucrose, 2.6 KCl, 1.23 NaH_2PO_4, 26 $NaHCO_3$, 10 glucose, 3 $MgCl_2.6H_2O$, and 1 $CaCl_2.2H_2O$, pH 7.35–7.4 (equilibrated with 95% O_2–5% CO_2), and blocked with an angle of ∼15°–20° from the horizontal plane (lateral raised; Fig. 1*B*). The brain block was then quickly moved into the holding chamber of a slicing microtome (Leica VT1200) containing icy-cold oxygenated dissecting solution. Two 400-µm-thickness thalamocortical slices were obtained and recovered in 30°C oxygenated artificial cerebrospinal fluid (ACSF, in mM): 130 NaCl, 3 KCl, 1.25 NaH_2PO_4, 20 $NaHCO_3$, 10 glucose, 1.3 $MgSO_4.7H_2O$, and 2.5 $CaCl_2.2H_2O$, pH 7.35–7.4 (equilibrated with 95% O_2–5% CO_2) for 45 min.

Electrophysiological recording. For all recordings, the thalamocortical slices were held in a chamber mounted on the fixed stage of a microscope (Olympus BX51) and recorded at room temperature (21–24°C) using borosilicate recording electrodes with input resistance of 5–12 MΩ (pulled by Sutter Instrument). Neurons expressing tdTomato reporter were identified under fluorescence (Thorlabs LED) with a 40× objective lens (Olympus) prior to whole-cell recordings. To recover the neuronal morphology of the cells recorded, the internal solution used in this study contained 0.5% biocytin. For all recordings, membrane voltages were corrected for an estimated liquid junction potential of 10 mV.

For general electrophysiological recording, the chamber was superfused with oxygenated ACSF at 2–4 ml/min. Whole-cell recordings were performed with recording pipettes filled with gluconate-based internal solution containing the following (in mM): 108 potassium gluconate, 2 KCl, 0.2 $CaCl_2.2H_2O$, 10 HEPES, 1 EGTA, 1.5 Na_2ATP, 0.3 Na_2GTP, 1 $MgCl_2.6H_2O$, and 5 glutathione, pH 7.25 (280 mOsm). To study the intrinsic membrane properties, the cells were recorded at the holding potential of −70 mV in the voltage-clamp mode and then switched to the current-clamp mode to characterize spiking properties. A square current pulse of 500 ms from −50 to 80 pA with 10 pA steps were applied. In some cases, the square current pulse was increased to

100 pA to elicit a spike. All recordings were made with a patch-clamp amplifier (MultiClamp 700B amplifier, Molecular Devices), digitized using a DAQ board (NI PCI-6259, National Instruments), and acquired using the WaveSurfer software (HHMI Janelia Farms).

For LSPS experiments, the recording chamber was superfused with oxygenated high-divalent ACSF (in mM), 124 NaCl, 5 KCl, 1.23 NaH_2PO_4, 26 $NaHCO_3$, 10 glucose, 4 $MgCl.6H_2O$, and 4 $CaCl_2.2H_2O$, to reduce polysynaptic transmission. The recording pipette was filled with a cesium-based internal solution containing the following (in mM): 115 cesium methanesulfonate ($CsCH_3SO_3$), 5 NaF, 10 EGTA, 10 HEPES, 15 CsCl, 3.5 MgATP, and 3 QX-314, pH 7.25 (300 mOsm). For photostimulation, ~0.5–1 mM caged glutamate [*N*-(6-nitro-7-coumarylmethyl)-L-glutamate; Kao, 2006] was added to the high-divalent ACSF solution. Without UV light, this compound does not have any effect on neuronal activity (Kao, 2006; Muralidharan et al., 2016). UV laser light (355 nm, 1 ms pulses, DPSS Lasers) was split by a 33% beam splitter (CVI Melles Griot), attenuated by a Pockels cell (Conoptics), gated with a laser shutter (NM Laser), and coupled into a microscope via scan mirrors (Cambridge Technology) and a dichroic mirror. The laser beam entered the slice axially through the objective (Olympus 10×, 0.3 NA/water) with a diameter of <20 μm. Laser power at the sample was adjusted to 25–26 mW. To ensure the photostimulation extended from the pial matter to the white matter of A1, at least 700 sites were stimulated, which enabled us to probe areas of ~1 mm^2. Stimuli were applied at 0.5–1 Hz, for such a dense sampling rate helped reduce the influence of spontaneous events. To record the excitatory or inhibitory postsynaptic currents (EPSPs or IPSCs), cells were recorded at the holding potentials of −70 and 0 mV, respectively. Series resistance was typically 20–40 MΩ and was not compensated during recording. Recordings were performed at room temperature and in high-Mg^{2+} solution to reduce the probability of polysynaptic inputs. All recordings were made with a patch-clamp amplifier (MultiClamp 700B amplifier, Molecular Devices), digitized using a DAQ board (NI PCI-6259, National Instruments), and acquired with a custom software (Ephus; Suter et al., 2010) written in MATLAB (MathWorks).

Biocytin staining and reconstruction of neuronal morphology. After recording, the thalamocortical slices were incubated in 4% paraformaldehyde (catalog #281692, Santa Cruz Biotechnology) at 4°C until biocytin staining. Biocytin staining was performed as previously reported (Zhao et al., 2009; Sheikh et al., 2019). Briefly, the thalamocortical slice was washed with 10 mM phosphate-buffered saline, pH 7.4 (catalog #P4417, Sigma-Aldrich), and then incubated with methanol/30% hydrogen peroxide solution ($v/v = 9{:}1$) for 30 min at room temperature to quench the endogenous peroxidase activity in the fixed slice. The slice was washed with 0.1 M phosphate buffer followed by 0.9% NaCl buffered with 50 mM Tris (TBS), pH 7.4, before blocking with TBS containing 2% Triton X-100 for 45 min at room temperature. Then, the slice was incubated overnight at 4°C with ABC reagent (catalog #PK-4000, Vector Laboratories) dissolved in TBS containing 0.05% Triton X-100. The next day, the slice was washed with 50 mM TBS and followed with 50 mM Tris buffer before being incubated in DAB solution (catalog #SK-4100, Vector Laboratories) for 30 min at room temperature in the dark. The slices were oxidized with hydrogen peroxide (catalog #SK-4100, Vector Laboratories) for 2–10 min until brown precipitate formed. All slices were processed with standard dehydration steps and xylene before being mounted with Permount (catalog #SP-15-500, Thermo Fisher Scientific). The neurons were traced under 40× or 100× magnification for neuronal morphology reconstruction with the Neurolucida software (MBF Bioscience) paired with a Zeiss AxioImager microscope. The traced neurons were analyzed using the Neurolucida software (MBF Bioscience).

Intrinsic properties analysis. Data were analyzed using a custom software written in MATLAB. The trials were averaged. Resting membrane potential was measured 500 ms before the stimulation started. The input resistance was determined using the slope of the *I–V* plot. For the active membrane properties, the traces containing the first spike were retrieved. The spike threshold was determined as the membrane potential at which the first derivative reached 10% of the overall peak first derivative. The amplitude of the first spike was measured from the threshold. All group data across different cell types and age groups were tested statistically with a Kruskal–Wallis test. If the Prob > *F* showed a significant difference ($p < 0.05$), a post hoc Bonferroni's test was performed across cell types and age groups to determine which means differed. All figures were plotted as means ± standard error of the mean (SEM).

LSPS analysis. Data were analyzed using a custom software written in MATLAB. Putative monosynaptic postsynaptic currents (PSCs) were classified by the poststimulation latency of the evoked current, as described previously (Meng et al., 2014, 2021; Sheikh et al., 2019). Traces with short latency (<8 ms) were discarded from the analysis because the responses are likely the result of direct activation of glutamate receptors on the recorded cell (Meng et al., 2014). Traces with longer latency (>50 ms) were discarded because of the potential involvement of polysynaptic components. Evoked currents with latencies between 8 and 50 ms were classified as monosynaptically evoked PSCs and were used for analysis in this study. In addition, cells that did not show any large (>100 pA) direct responses were excluded from the analysis, as these could be astrocytes. For each cell, the input area was calculated as the area that gave rise to direct synaptic inputs. The charge (the area of EPSC in the counting window) was quantified for each synaptic response. The mean input area and charge was the average of the respective input area and charge of PSCs from each stimulus spot. A spatial connectivity map was calculated by aligning the somata of the monitored neurons and calculating the fraction of cells that provided input at each spatial location (Figs. 2, 3). To evaluate the contribution of synaptic inputs from each lamina, the cortex was divided into five laminas (i.e., L1–L3, L4, L5, L6, SP/L6b) by features in the bright-field image based on the laminar proportions reported previously (Chang et al., 2018). The balance of excitation and inhibition was calculated as the *E*/*I* balance index, which is based on the average input strength $[(E-I)/(E+I)]$. This calculation results in a number that varies between −1 and 1, with 1 indicating dominant excitation and −1 indicating dominant inhibition (Meng et al., 2021; Mukherjee et al., 2022). Since the measurement of *E* is not possible close to the soma due to direct responses, the *E*/*I* measure does not account for the contribution of cells from nearby locations. All group data across different cell types and ages were tested statistically with the Kruskal–Wallis test (Figs. 2, 3). If the Prob > *F* showed a significant difference ($p < 0.05$), a post hoc Bonferroni's test was performed across cell types and age groups to determine which means differed. The data are plotted as means ± SEM (Figs. 2, 3).

For the rostral–caudal analysis, a binary connection map was generated based on the stimulus locations that showed evoked PSC. Then, 80% of the spatial inputs on the rostral–caudal axis were used to plot the graph indicated by the patch pattern, while the line plot indicates the center point of 80% of the spatial inputs. The recorded neurons were used as a center point (marked as "0"); any inputs located at the left side (−500 to 0) are interpreted as rostral, while those located at the right side (0–500) are considered caudal to the recorded neurons.

For the circuit similarity analysis, the pairwise correlation of the connection probability map within each subtype and their respective age groups were calculated. The correlation coefficient for each molecular class and age group was tested using the Kruskal–Wallis statistical test. If the Prob > *F* showed a significant difference ($p < 0.05$), a post hoc Bonferroni's test was performed across cell types and age groups to determine which means differed. For generating the Fano factor map, we calculated the Fano factor of the PSC as σ^2/μ for each responsive spatial location (Meng et al., 2021).

To categorize different classes of SpNs expressing CTGF and Drd1, *k*-means clustering was used on all maps between P7 and P80 (Meng et al., 2017). Clustering was done based on both columnar and percent cortical extent of spatial inputs at −70 mV. To determine the optimal number of clusters, the fraction of variance that the clusters explained (R^2) or the Dunn index was calculated for the numbers of clusters from 1 to 8.

Neuron morphology analysis. To categorize the reconstructed neurons, we used several criteria (Hanganu et al., 2002; Hoerder-Suabedissen and Molnár, 2012; Marx et al., 2017): (1) pyramidal,

neurons with a vertically oriented apical main dendrite with a distinct orientation toward the pial surface; (2) multipolar, neurons with no dominant apical or "apical-like" main dendrite and their dendrites projected in no preferred direction (this cell type showed the highest total dendrite length); (3) horizontal, neurons with a horizontally oriented "apical-like" main dendrite extending from the soma, parallel to the white matter; and (4) Inverted-pyramidal, neurons with an atypically oriented "apical-like" main dendrite which often extended toward the white matter.

To analyze the location of reconstructed neurons, the slice was imaged under 10× magnification (Olympus BX53 with Thorlabs Kiralux 12.3 MP Monochrome CMOS camera), and the images were processed using the Fiji software (ImageJ). The contours for the pial surface and L6/white matter border were traced and superimposed on the traced neurons, as shown in Figure 5. The *x*- and *y*-coordinates of the recorded neurons, pial surface, and L6/white matter border were marked. The distance between recorded neurons and the L6/white matter border was calculated.

The complexity of dendritic processes was calculated through the following equation [complexity = (sum of the terminal orders + number of terminals) × (total dendritic length / number of primary dendrites)] derived from the dendritic complexity index (Pillai et al., 2012). The statistical differences for all group data across different cell types and age groups were tested with the Kruskal–Wallis test. If the Prob > *F* showed a significant difference ($p < 0.05$), a post hoc Bonferroni's test was performed across cell types and age groups to determine which means differed. The data were plotted as mean ± SEM. We also performed Sholl analysis on the reconstructed neurons using the Neurolucida software (MBF Bioscience) to study the complexity of the neurons. Briefly, the 3D space surrounding the cell body was separated into 3D shell-like compartments of 5 µm thickness. The number of intersections of basal and apical dendrites within each compartment was counted, and then the number of intersections for every 25 µm was summed and plotted against the distance from the soma. For statistical comparison between the SpNs subtypes, a rank-sum test was used. All figures were plotted as mean ± SEM.

Results

The subplate comprises different subtypes of SpNs with distinct molecular identities (Hoerder-Suabedissen et al., 2009; Hoerder-Suabedissen and Molnár, 2013). The distribution of these molecular subclasses differs across the sensory cortices (Chang et al., 2024). For example, during the first three postnatal weeks, the ACtx contains more CTGF- than Drd1-expressing neurons (Chang et al., 2024). We sought to investigate the functional differences between the different molecular types of SpNs in the ACtx. In the somatosensory cortex, the Drd1 population consists of L6b neurons projecting to L1 (located within ∼100 µm from the white matter border) and corticothalamic neurons projecting to the thalamus (above ∼100 µm from the white matter border; Kim et al., 2024). Our prior anatomical comparison study across sensory cortices has demonstrated that these genetically labeled neurons are restricted to within 100 µm of the border of white matter in the ACtx compared with somatosensory and visual cortices (Chang et al., 2024; Fig. 1*C*). Thus, we here restricted our study to neurons within 100 µm of the border of white matter. This provided specificity in the selection of the recorded cells, ensuring that no other neurons residing outside the subplate or L6b were included in our study. To explore whether molecularly defined SpNs share distinct cortical connectivity and undergo changes with age, we aimed to study the electrophysiological properties and functional circuits of SpNs in the ACtx before and after the presence of peripheral auditory inputs (i.e., P7–P9, P14–P20, and P60–P80; Fig. 1*A*). To target specific cell types, we expressed tdTomato fluorescent reporter in these subsets of SpNs: (1) CTGF-tdTomato or (2) Drd1-tdTomato (Fig. 1*B*). For ease of reading, we will refer to these SpNs as CTGF and Drd1 neurons, respectively. For consistency, we chose to label CTGF and Drd1 neurons as SpNs during the first 3 postnatal weeks and as L6b at P60–P80, following the nomenclature used in previous studies (Piñon et al., 2009; Hoerder-Suabedissen and Molnár, 2012; Zolnik et al., 2020; Ghezzi et al., 2021; Kim et al., 2024). The lamina lying between L5 and subplate/L6b, comprised of L6 corticothalamic neurons (or L6a), were termed as L6 at all examined ages.

CTGF and Drd1 SpNs have similar intrinsic properties during the first 3 postnatal weeks

The intrinsic membrane properties of SpNs progressively mature during the first 2 postnatal weeks in rodents (Zhao et al., 2009; Liao and Lee, 2012). However, it is unclear whether different molecular types of SpNs share similar membrane properties and if they mature on a similar timeline. Therefore, we first performed whole-cell current–clamp recordings on SpNs in thalamocortical brain slices that contained both medial geniculate body (MGB) and A1 at P7–P9 (CTGF, 22 cells; Drd1, 21 cells) and P14–P20 (CTGF, 23 cells; Drd1, 20 cells; Fig. 1*D*). Upon a series of current injections, both subtypes of SpNs were capable of firing overshooting action potentials at both time points. Figure 1*E* showed an exemplar voltage traces from CTGF (blue) and Drd1 neurons (red). We characterized the membrane resistance, resting potential, spike threshold, and spike amplitude. There were no significant differences in the passive and active membrane properties between the two subtypes at both examined age groups (Fig. 1*F–I*). When comparing the P7–P9 and P14–P20 age groups, the resting membrane potential was slightly more depolarized in the younger age group, and the input resistance declined with age for both CTGF and Drd1 neurons (Fig. 1*F*,*G*; $p < 0.05$; Kruskal–Wallis test with post hoc Bonferroni's). This developmental maturation of the passive membrane properties is consistent with prior results (Zhao et al., 2009; Liao and Lee, 2012). For the active membrane properties, we analyzed the first evoked action potential in each recording. The spike threshold became more negative from P7–P9 to P14–P20 for both subtypes (Fig. 1*H*), and the amplitude of the spikes increased with age (Fig. 1*I*; $p < 0.05$; Kruskal–Wallis test with post hoc Bonferroni's). The intrinsic properties of excitatory and inhibitory neurons in the L2/3 of the ACtx mature ∼P19 (Oswald and Reyes, 2008, 2011). Since SpNs are born earlier and since most of these neurons achieve maturation or die off during the first 3 postnatal weeks (Hoerder-Suabedissen and Molnár, 2013), we speculated that their membrane properties would not change after the third postnatal week into adulthood. To confirm this speculation, we recorded L6b neurons at P60–P80 (eight CTGF and six Drd1 neurons). The intrinsic properties for both subtypes of L6b neurons at P60–P80 (V_{rest}, CTGF = −63.44 ± 2.58 mV; Drd1 = −57.81 ± 2.8 mV; R_{in}, CTGF = 318.15 ± 25.12 MOhm; Drd1 = 340.26 ± 20.27 MOhm; threshold, CTGF = −38.55 ± 0.62 mV; Drd1 = −35.86 ± 1.06 mV; amplitude, CTGF = 77.62 ± 5.06 mV; Drd1 = 79.74 ± 2.22 mV) were similar to their respective age groups at P14–P20 ($p > 0.05$; Kruskal–Wallis test with post hoc Bonferroni's), indicating that intrinsic properties did not change after the third postnatal weeks. Additionally, there were no significant differences between the two subtypes at P60–P80 ($p > 0.05$; Kruskal–Wallis test with post hoc Bonferroni's). Overall, these results demonstrate that SpNs of both molecular classes show similar passive and active membrane properties. Both types of SpNs progressively mature from the second to third postnatal week and that intrinsic properties remain stable to adulthood.

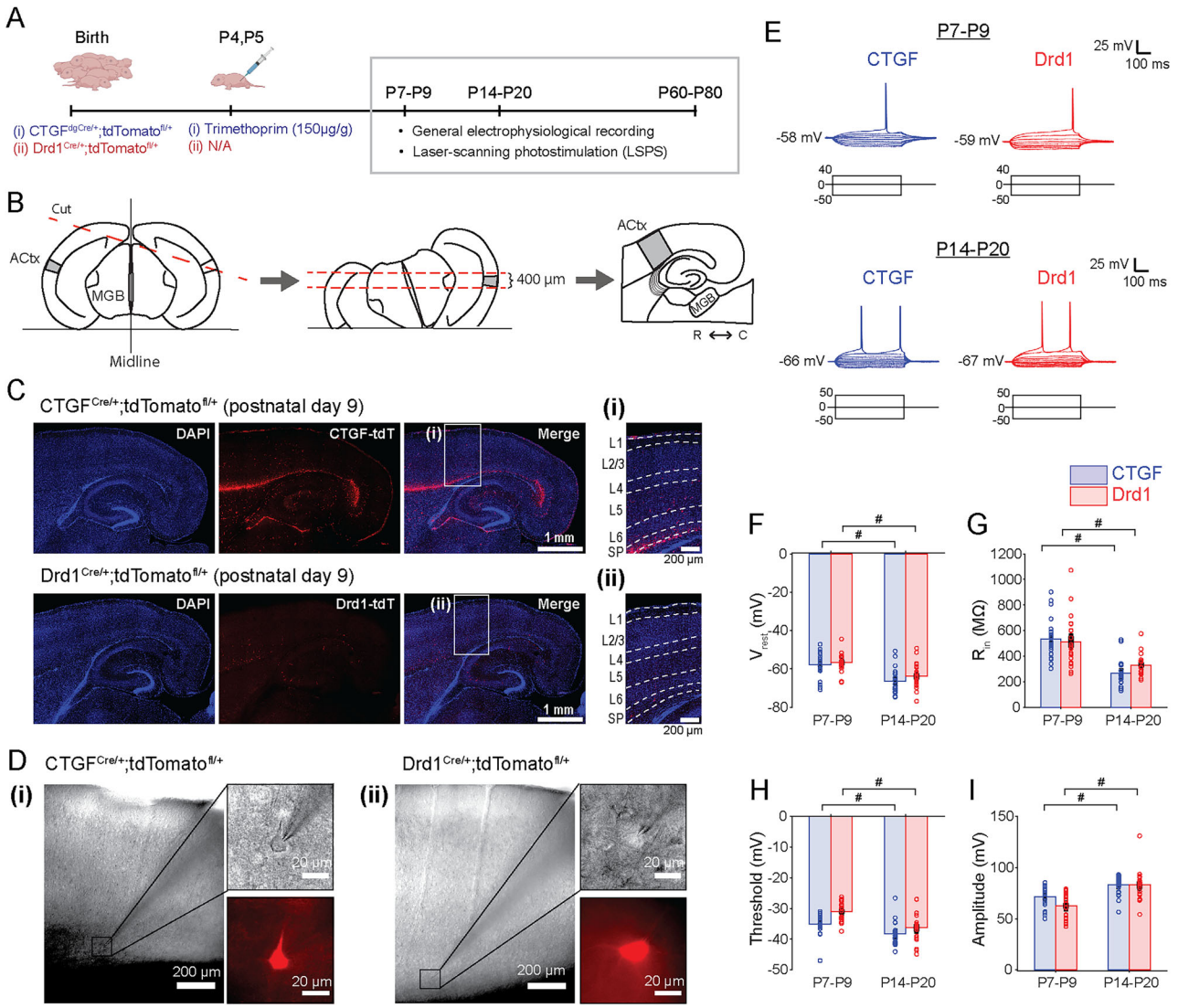


Figure 1. Membrane properties of CTGF and Drd1 neurons. ***A***, Schematic of experimental procedures. ***B***, Schematic of auditory thalamocortical slice preparation. Left, The brain is blocked at an angle of ~15–20° from the horizontal plane (lateral raised, as indicated by the red dotted line). Middle, Right, A 400 μm thickness of thalamocortical slice containing ACtx and the ventral division of MGB is obtained for recording. R, rostral; C, caudal. ***C***, Representative images of thalamocortical slices for CTGF- (top) and Drd1- (bottom) expressing tdTomato reporter expression stained with nuclear marker, DAPI. Scale bar, 1 mm. The white box is magnified on the right for CTGF (***i***) and Drd1 (***ii***). Scale bar, 200 μm. ***D***, Representative images of thalamocortical slices under bright-field illumination for whole-cell patch recording are shown on the left. Scale bar, 200 μm. The black box is magnified in the top-right for CTGF (***i***) and Drd1 (***ii***) neurons, with their tdTomato reporter expression shown in the bottom-right. Scale bar, 20 μm. ***E***, Example of traces for the first detected spikes in CTGF (blue) and Drd1 (red) neurons at P7–P9 (left) and P14–P20 (right). ***F–I***, Comparison of resting membrane potential (V_{rest}, ***F***), input resistance (R_{in}, ***G***), threshold (***H***), and the amplitude of first action potential (***I***) between CTGF (blue) and Drd1 neurons (red). Each circle represents data from a neuron. All data are represented as mean ± SEM. Symbols indicate $p < 0.05$ with Kruskal–Wallis test with post hoc Bonferroni's correction. # compares between P7–P9 and P14–P20. P7–P9, CTGF = 22 cells; Drd1 = 21 cells. P14–P60, CTGF = 23 cells; Drd1 = 20 cells.

CTGF and Drd1 SpNs receive more intracortical inputs from the lower layers and prune with age

SpNs receive synaptic inputs from within the subplate and from other cortical layers, and the spatial pattern of laminar inputs changes over time during the first 2 postnatal weeks (Viswanathan et al., 2012; Meng et al., 2014). We thus investigated if functional connections to each subtype of SpNs develop differently by performing whole-cell voltage–clamp recordings coupled with LSPS (Shepherd et al., 2003). Since many SpNs survive to adulthood and form L6b in rodents (Valverde et al., 1995; Clancy et al., 2001), we also recorded L6b neurons in adult mice. Again, we restricted our study to neurons within 100 μm of the border of white matter to exclude L6a neurons. Prior cell-attached recordings under identical conditions have demonstrated that neurons ranging from P4 to 1-year-old mice located across cortical L2–6 and within the subplate/L6b of the ACtx are capable of firing action potentials in response to photo-released glutamate and that the spatial resolution of LSPS remained stable with age (Viswanathan et al., 2012; Meng et al., 2014, 2021; Xue et al., 2023). We thus mapped CTGF and Drd1 neurons targeting three different time windows: P7–P9 (CTGF, 24 cells; Drd1, 28 cells), P14–P20 (CTGF, 23 cells; Drd1, 33 cells), and P60–P80 (CTGF, 24 cells; Drd1, 28 cells).

To record the evoked excitatory synaptic currents, cells were held at −70 mV; to record inhibitory synaptic currents, cells were held at 0 mV (Fig. 2*A*). For each cell and each stimulation site, we identified if the cell received a synaptic input (see Materials and Methods) and generated binary connection maps (one excitatory and one inhibitory) for each cell, which indicate the stimulus locations providing input to the cell (Fig. 2*Aiii*,*iv*). The soma of

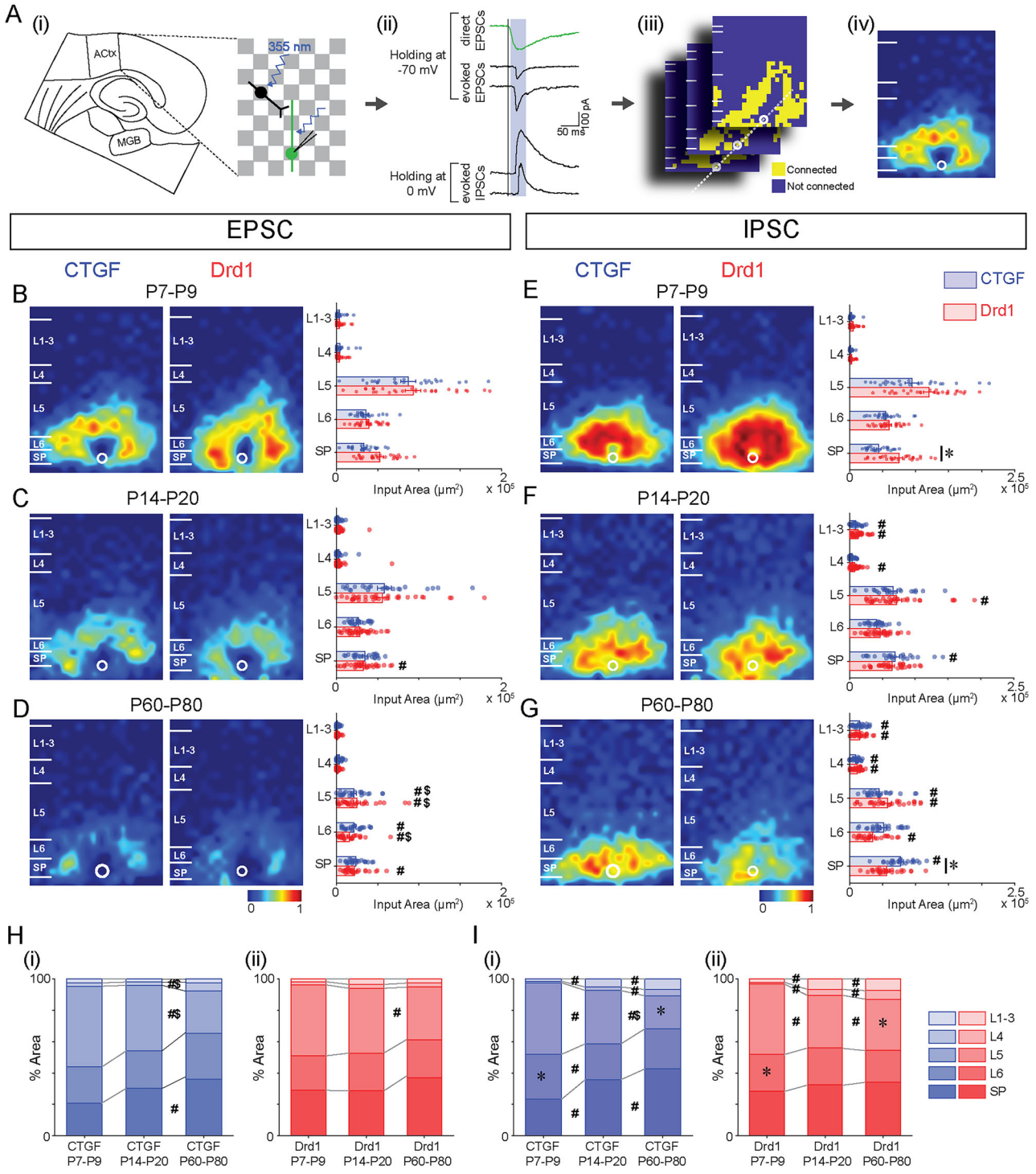


Figure 2. Fraction of intracortical inputs on CTGF and Drd1 neurons. ***A***, Schematic of LSPS experiment and analysis. ***i***, Schematic of the thalamocortical slice with a whole-cell patched neuron (green) coupled with LSPS. Multiple stimulation spots (gray and white) are randomly activated by a UV laser (355 nm). ***ii***, Example traces of direct EPSCs (green), evoked EPSCs, and evoked IPSCs. ***iii***, ***iv***, Schematic of aligning binary connection maps of each cell based on the patched cell location to generate average connection maps. ***B–G***, A two-dimensional connectivity map indicating the probability of connection for EPSC (***B–D***) and IPSC (***E–G***) from L1–6 and subplate (SP) onto CTGF (blue) and Drd1 (red) neurons at P7–P9 (***B***, ***E***), P14–P20 (***C***, ***F***), and P60–P80 (***D***, ***G***). Darker blue (1) indicates a lower probability of connection to the site of stimulation onto the recorded neurons (white circle), while darker red (0) indicates the opposite. The bar plots represent the averaged input area of all recorded neurons, while each circle represents the laminar input area for a single map. ***H***, ***I***, Fraction of laminar inputs onto recorded CTGF (***i***, blue) and Drd1 neurons (***ii***, red) for EPSC (***H***) and IPSC (***I***). All data are represented as mean ± SEM. Symbols indicate $p < 0.05$ with Kruskal–Wallis test with post hoc Bonferroni's correction. * compares between CTGF and Drd1. # compares between P14–P20 and P60–P80 with P7–P9. $ compares between P14–P20 and P60–P80. P7–P9, CTGF = 24 cells; Drd1 = 28 cells. P14–P60, CTGF = 23 cells; Drd1 = 33 cells. P60–P80, CTGF = 24 cells; Drd1 = 28 cells.

the recorded cells in each age group was aligned, and a spatial connection probability map was generated by averaging the inputs at each stimulus site across cells. This map indicates, for each stimulus location, the fraction of cells that receive inputs from this particular stimulus location. At P7–P9, both CTGF and Drd1 neurons receive abundant excitatory (left panel) and

inhibitory (right panel) input from within the subplate but also input from the other cortical layers, including L4 (Fig. 2*B*,*E*), consistent with prior observations (Viswanathan et al., 2012). Inspection of these maps in the different age groups showed that the probability of an evoked excitatory and inhibitory synaptic event decreases with age, as indicated in the pseudocolor maps at P14–P20 (Fig. 2*C*,*F*) and at P60–P80 (Fig. 2*D*,*G*). These results show that both subtypes of SpNs receive abundant intracortical inputs and that these inputs change with age.

CTGF and Drd1 SpNs share similar excitatory intracortical input patterns across age

The decrease in the connection probability map with age can be due to a decrease in connection or diversification of the inputs with age. If all the maps of individual cells were identical, the average spatial connectivity map would have a connection probability of 1 wherever there is an overlap. However, if all the maps are very different but still have some overlaps, even if each map still has the same number of inputs, the average spatial connectivity map would show a lower connection probability in the overlapping areas. To first test if the amount of inputs decreased with age, we quantified the contribution of synaptic inputs from each cortical lamina on each SpN. For each cell, we calculated the area within each layer that provided inputs to the SpN. The measurement reflects the number of synaptic connections from each cortical layer to the recorded neuron (bar plots in Fig. 2*B–D* for EPCSs and Fig. 2*E–G* for IPSCs). The excitatory input areas to CTGF and Drd1 neurons were mostly similar, except that there was a tendency of more excitatory synaptic connections from within the subplate on Drd1 compared with CTGF neurons at P7–P9 ($p = 0.0544$; Kruskal–Wallis test with post hoc Bonferroni's). In addition, both subtypes showed pruning in excitatory synaptic connections with age, especially those from lower layers to SpNs (Fig. 2*B–D*, bar plots). The amount of excitatory synaptic connections from L5 on CTGF neurons declined by ∼76% ($p = 0.01$), and L5 input to Drd1 neurons declined by 73% ($p < 0.0001$) at P60–P80 compared with P7–P9 (Fig. 2*D*, #). The amount of excitatory synaptic connections from L6 also showed a decline of 40% for CTGF ($p = 0.03$) and 59% for Drd1 neurons ($p < 0.0001$; Fig. 2*D*, #). In contrast, the amount of excitatory synaptic connections within the L6b on Drd1 neurons at P60–P80 showed a decline of 58% ($p < 0.0001$), while those on CTGF neurons showed no significant changes when comparing with their respective younger age groups ($p = 0.22$; Kruskal–Wallis test with post hoc Bonferroni's; Fig. 2*D*, #). Although there were no statistical differences between the two subtypes at all examined ages, the developmental trends suggest that the excitatory synaptic connections within the subplate/L6b on CTGF neurons likely reach a steady state by P7, while those on Drd1 neurons continue to decline to adulthood. Overall, when comparing the two subtypes, the excitatory synaptic inputs from L1–L3, L4, L5, and L6 and within subplate/L6b to CTGF and Drd1 neurons were similar at all examined age groups. These results suggest that overall excitatory intracortical connection to both types of SpNs largely develops similarly and reduces into adulthood.

CTGF and Drd1 SpNs differ in inhibitory intracortical patterns across age

We next analyzed the maturation of intracortical inhibitory inputs to SpNs. In contrast to the largely similar amounts of excitatory inputs to CTGF and Drd1 neurons, inhibitory inputs showed large differences between SpN classes. There were more inhibitory synaptic connections from within the subplate on Drd1 ($7.4 \pm 0.5 \times 10^4$ μm^2) when compared with CTGF neurons ($4.4 \pm 0.3 \times 10^4$ μm^2; $p < 0.001$; Kruskal–Wallis test with post hoc Bonferroni's) at P7–P9 (Fig. 2*E* bar plots). Such differences were not obvious at P14–P20 (Fig. 2*F*). However, at P60–P80, an opposite relationship was observed where there were more inhibitory connections to CTGF ($7.7 \pm 0.4 \times 10^4$ μm^2) than Drd1 neurons ($5.6 \pm 0.4 \times 10^4$ μm^2; $p = 0.011$, Kruskal–Wallis test with post hoc Bonferroni's; Fig. 2*G*). This is likely due to a developmental change in CTGF neurons where there were more synaptic connections from within the subplate at P14–P20 compared with their respective younger age group (P7–P9, $7.0 \pm 0.7 \times 10^4$ μm^2; $p = 0.003$; Kruskal–Wallis test with post hoc Bonferroni's; Fig. 2*F*), while such developmental changes were not found in Drd1 neurons. In addition, at P60–P80, there was a trend of a higher amount of inhibitory synaptic inputs from L6 on CTGF ($5.1 \pm 0.5 \times 10^4$ μm^2) than that on Drd1 neurons ($3.4 \pm 0.4 \times 10^4$ μm^2; $p = 0.058$; Kruskal–Wallis test with post hoc Bonferroni's; Fig. 2*G*). We also found the amount of inhibitory synaptic connections from L1–3 and L4 on CTGF neurons increased by 5.4-fold, while those connections from L1–3 and L4 on Drd1 neurons increased only by 2.7-fold and 3.8-fold, respectively ($p < 0.05$; Kruskal–Wallis test with post hoc Bonferroni's). However, the amount of inhibitory synaptic connections from L5 prunes by ∼52% between P7–P9 and P60–P80 for both CTGF and Drd1 neurons ($p < 0.001$; Kruskal–Wallis test with post hoc Bonferroni's). The amounts of inhibitory connections from L6 on both CTGF and Drd1 neurons at P60–P80 did not change significantly from P7–P9 for each respective subtype. In contrast, the developmental trajectories of inhibitory synaptic connections from within the subplate/L6b to CTGF and Drd1 neurons were opposite; there were no significant changes between P7–P9 and P60–P80 for Drd1 neurons but an increase of ∼25% of synaptic connections on CTGF subtypes (Fig. 2*E*,*G*). Together, these results show that the molecular subtypes of SpNs receive similar excitatory intracortical connectivity patterns during development but not inhibitory intracortical connections. Not only do these subtypes have different amounts of inhibitory inputs, their intracortical connectivity also develops in a lamina-dependent manner.

The changes in laminar inputs suggested that the balance of inputs from each lamina changes with development. Thus, we measured the fraction of inputs provided by each layer (total input area from each cortical layer divided by the total input area; Fig. 2*H*,*I*). At P7–P9, the largest relative input area contributing to the excitatory synaptic events on recorded CTGF and Drd1 neurons mostly comes from L5 (CTGF, ∼51%; Drd1, ∼45%), followed by L6 (CTGF, ∼23%; Drd1, ∼22%) and SP (CTGF, ∼21%; Drd1, ∼29%; Fig. 2*H*). Similarly, the relative input areas contributing to the inhibitory synaptic events on a recorded CTGF (L5, ∼46%; L6, ∼29%; SP, ∼23%) and Drd1 neurons are mainly from the lower layers (L5, ∼45%; L6, ∼24%; SP, ∼28%; Fig. 2*I*). At P14–P20, the fraction of input area that showed synaptic connections with recorded CTGF neurons (EPSCs, ∼96%; IPSCs, 93%) and Drd1 neurons (EPSCs, ∼94%; IPSCs, 90%) are still mainly from the lower layers (Fig. 2*H*,*I*). Such proportion of spatial intracortical input retained to adulthood for CTGF (EPSCs, ∼92; IPSCs, 87%) and Drd1 (EPSCs, ∼95%; IPSCs, ∼86%; Fig. 2*H*,*I*). In addition, our analysis showed an increase in the proportion of inhibitory connection from upper layers (L1–3 and L4) to both subtypes increases with age (P7–P9→P14–P20→P60–P80; CTGF, 2.2→7.3→12.7%; Drd1, 3.1→10.3→14.3%; Fig. 2*I*). Cortical maturation in the upper

layers in the ACtx is still ongoing during the first 2 postnatal weeks (Chang et al., 2018). During this period, the thalamocortical inputs are refined in L4 (Barkat et al., 2011), and the excitatory and inhibitory neurons in L2/3 are maturing (Oswald and Reyes, 2008, 2011). We speculate that the increase in the inhibitory connection from the upper layers reflects the maturation of inhibitory connectivity, which coincides with the opening of the critical period (Takesian et al., 2018). Overall, our analysis showed that CTGF and Drd1 neurons received more excitatory and inhibitory inputs from L5 and L6 and within the subplate compared with the upper layers for each age group. Our results also showed that CTGF and Drd1 neurons differed more in their inhibitory than excitatory inputs.

CTGF and Drd1 SpNs show differences in the strength of inhibition

So far, we have shown that CTGF and Drd1 neurons differ in the amounts of intracortical input they receive from the different cortical layers. Differences in neural connectivity can be manifested in the number of connections as well as changes in the strength of connections. Thus, we next quantified the synaptic strength from each stimulus location by calculating the average transferred charge of the EPSCs from each stimulus location and the averaging across all locations within each layer (Fig. 3). From the two-dimensional maps, a decrease in the EPSC charge with age was noticeable for both SpN subtypes (Fig. 3*A–C*). The excitatory synaptic strength from each cortical layer on CTGF

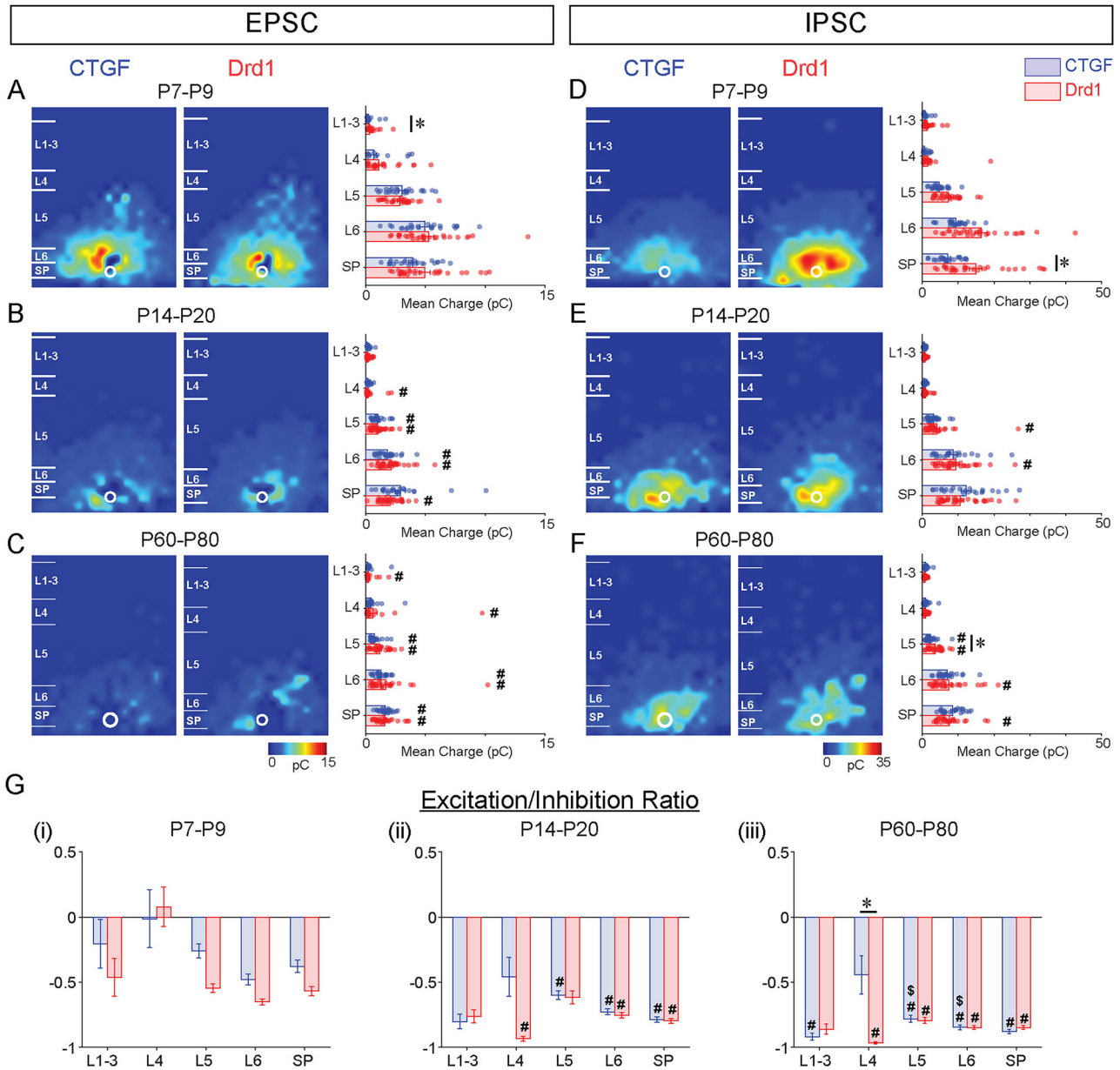


Figure 3. Evoked excitatory and inhibitory synaptic strength onto CTGF and Drd1 neurons. ***A–F***, Two-dimensional connectivity map indicating the transferred charge (pC) for EPSC (***A–C***) and IPSC (***D–F***) from L1–6 and subplate (SP) onto CTGF (blue) and Drd1 (red) neurons at P7–P9 (***A***, ***D***), P14–P20 (***B***, ***E***), and P60–P80 (***C***, ***F***). Darker blue (0 pA) indicates weaker synaptic inputs from the site of stimulation onto the recorded neurons (white circle), while darker red (15 or 35 pA) indicates the opposite. The bar plots represent the average transferred charge of all recorded neurons, while each circle represents the transferred charge for a single map. ***G***, *E/I* ratio of transferred charge for CTGF (blue) and Drd1 (red) at different age groups. All data are represented as mean ± SEM. Symbols indicate $p < 0.05$ with Kruskal–Wallis test with post hoc Bonferroni's correction. * compares CTGF and Drd1. # compares P14–P20 and P60–P80 with P7–P9. $ compares P14–P20 and P60–P80. P7–P9, CTGF = 24 cells; Drd1 = 28 cells. P14–P60, CTGF = 23 cells; Drd1 = 33 cells. P60–P80, CTGF = 24 cells; Drd1 = 28 cells.

and Drd1 neurons were similar at P7–P9, except for those from L1–3 (CTGF, 0.2 ± 0.1 pC; Drd1, 0.3 ± 0.1 pC; $p = 0.04$; Kruskal–Wallis test with post hoc Bonferroni's). Although the area of connections was similar (Fig. 2*B*), the average transferred charge was higher in the Drd1 than in CTGF neurons (Fig. 3*A*), suggesting stronger excitatory synaptic connections from L1–3 neurons to Drd1 SpNs. Such differences disappear at the third postnatal week, and the subpopulations remain similar into adulthood (Fig. 3*B*,*C*). Developmentally, for both CTGF and Drd1 SpNs, the synaptic strength decreases for all cortical layers from P7–P9 to P60–P80 ($p < 0.05$; Kruskal–Wallis test with post hoc Bonferroni's; Fig. 3*A*,*C*).

The inhibitory synaptic input strength to CTGF and Drd1 neurons, on the other hand, showed different developmental patterns from the excitatory inputs. From the two-dimensional maps, it is noticeable that for CTGF neurons, there is an increase of transferred charge between P7–P9 and P14–P20 and then a decrease at P60–P80, while for Drd1 neurons, the transferred charge continuously decreased from P7–P9 to P60–P80 (Fig. 3*D*–*F*). Quantitative analysis showed that such changes were lamina-dependent (Fig. 3*D*–*F*, bar plots). The synaptic strength from L1–3 and L4 on CTGF and Drd1 neurons did not change during development (Fig. 3*D*–*F*), although the number of connections (Fig. 2*E*–*G*) increased from P7–P9 to P60–P80. The synaptic strength from L5 neurons on CTGF and Drd1 neurons decreased from P7–P9 to P60–P80 (CTGF, 4.7 ± 0.4 pC→2.2 ± 0.3 pC; $p = 0.0001$; Drd1, 7.2 ± 0.7 pC→3.6 ± 0.4 pC; $p = 0.002$). The synaptic connection strength from L6 on CTGF neurons remained similar from P7–P9 (9.4 ± 0.7 pC) to P60–P80 (6.8 ± 0.6 pC; $p = 0.08$). Meanwhile, the synaptic strength on Drd1 neurons decreased significantly from P7–P9 (16.4 ± 1.7 pC) to P14–P20 (9.5 ± 0.9 pC; $p = 0.02$) and then remained similar at P60–P80 (7.4 ± 1.0 pC; Fig. 3*D*–*F*, bar plots). At P7–P9, inhibition from within the subplate was stronger on Drd1 neurons (14.9 ± 1.7 pC) than on CTGF neurons (7.2 ± 0.6 pC, $p = 0.004$, Kruskal–Wallis test with post hoc Bonferroni's; Fig. 3*D*). Such differences were less obvious at P14–P20, as there was a slight increase of synaptic strength on CTGF neurons (12.2 ± 1.4 pC; $p = 1$; Kruskal–Wallis test with post hoc Bonferroni's; Fig. 3*E*). At P60–P80, inhibition on both neurons declined to similar levels (Fig. 3*F*). Overall, these results suggest that different molecular subgroups of SpNs are integrated differently into the cortical circuits and thus likely play different functional roles, especially during development.

SpNs receive relatively more excitatory inputs from L4 during the first postnatal weeks but L4 inputs in Drd1 neurons became relatively more inhibitory in adults when compared with CTGF neurons

So far, we have analyzed the strength of excitatory and inhibitory synaptic inputs from each layer separately (Fig. 3). Our analysis showed that the spatial and temporal patterns for both excitatory and inhibitory circuits change differently over development for both subtypes of SpNs. The net effect of activity in each layer depends on the balance of excitation and inhibition; thus, we calculated the *E*/*I* balance index $[(E-I)/(E+I)]$ based on the mean charge for the laminar inputs on CTGF and Drd1 neurons (Meng et al., 2015, 2017, 2020, 2021). A positive *E*/*I* balance index toward 1 indicates the neurons received excitation-dominant inputs, while a negative index toward −1 indicates the neurons received inhibition-dominant inputs. At P7–P9, the *E*/*I* index is negative for inputs from all layers except Layer 4, indicating a relative paucity of inhibitory inputs and relatively stronger excitation from L4 (Fig. 3*G*). With age, the *E*/*I* index in L4 for both subtypes became more inhibition-dominant, especially for Drd1 neurons (Fig. 3*Gii*). The switching from excitation-dominant to inhibition-dominant is likely due to the maturation of inhibitory neurons in the upper layers (Oswald and Reyes, 2011) and the strengthening of thalamocortical inputs on L4 neurons with the ear-canals opening (Barkat et al., 2011). Although the L4 *E*/*I* index of CTGF and Drd1 neurons were not significantly different at this time point (P14–P20, $p = 0.057$), the *E*/*I* index in L4 was more negative for Drd1 than CTGF neurons in adults ($p < 0.05$ Kruskal–Wallis test with post hoc Bonferroni's; Fig. 3*G*, right). Together, these results suggest that CTGF and Drd1 SpNs show differences with respect to their balance of excitatory and inhibitory input strength, especially from L4 at older ages. Moreover, our results show that both subgroups receive relatively more excitatory input from L4 than any other layer at young ages.

Upper layers inputs on SpNs are biased to originate from the caudal direction during the early postnatal period, but not in adult

We performed our recordings in thalamocortical slices; such that the rostrocaudal direction (tonotopic organization) is preserved in the slice (left–right in the 2D maps). From the spatial connection probability map (Fig. 2), we noticed relatively more upper layer inputs originating from the right (caudal) side of the recorded neurons. To quantitatively examine whether the SpNs potentially receive intracortical inputs in a spatially biased manner, we analyzed the spatial range of inputs, which accounts for 80% of responses along the tonotopic (rostrocaudal) axis (see Materials and Methods). At P7–P9, the averaged excitatory and inhibitory inputs from the upper layers (>500 μm) on CTGF and Drd1 neurons are biased to the right (caudal) direction, but such a bias is not present for inputs from the lower layers (<500 μm; Fig. 4*Ai*,*Bi*). This pattern of the bias remained at P14–P20, but the spatial range of intracortical inputs from the upper layers now shifted more toward the center (Fig. 4*Aii*,*Bii*). In the adult, the excitatory inputs on CTGF neurons from the area between ∼700 and 900 μm (likely L2) were biased to the rostral direction, while the inputs from the area between ∼500 and 700 μm were biased to the caudal direction (Fig. 4*Aiii*). Meanwhile, our analysis of Drd1 neurons indicated that inputs from the mid-upper layers (between ∼500 and 900 μm) were biased to the rostral direction (Fig. 4*Aiii*). In contrast, the inhibitory inputs to both CTGF and Drd1 neurons from each layer were distributed evenly between the rostral and caudal directions (Fig. 4*Biii*). The term cortical "column" is ambiguous and can refer to structures ranging from small-scale columns (∼50 μm in diameter) to larger-scale columns (∼300–500 μm in diameter; Jones, 2000; Rockland, 2010). Our analysis shows that the integration of other cortical inputs on SpNs/L6b neurons remains confined within a radial column of 0–500 μm throughout development. While the excitatory inputs from the upper layers exhibit a developmental remodeling from the caudal direction toward the rostral direction, the inhibitory inputs shift from the caudal direction toward the center. Despite these shifts, the process remains within a columnar organization. Additionally, such developmental changes were observed, especially after the ear canals opened, suggesting the peripheral inputs likely shape this process.

The dendritic processes of CTGF SpNs are more complex than those of Drd1 SpN at P14–P20, but not in the adult

Previous studies have demonstrated a variation in neuronal morphology among SpNs (Wahle et al., 1987; Valverde and Facal-Valverde, 1988; deAzevedo et al., 1997; Robertson et al.,

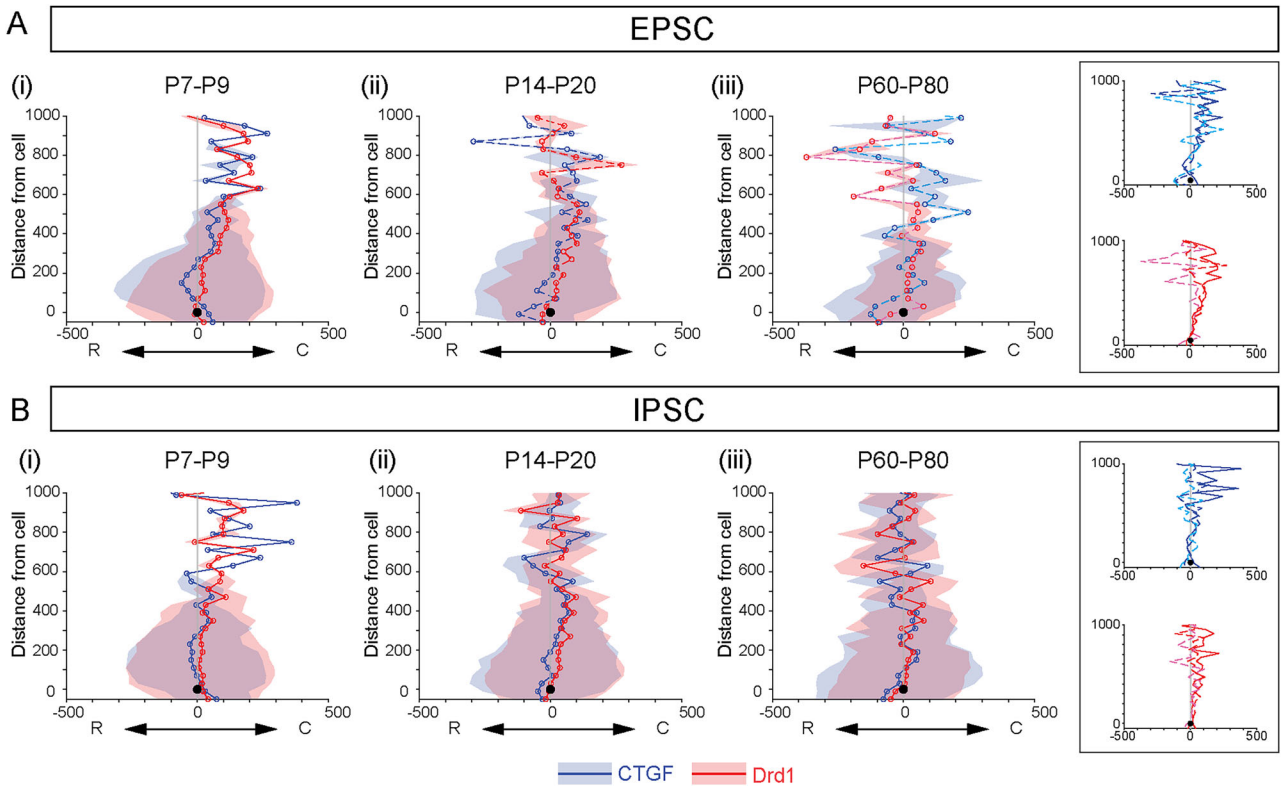


Figure 4. SpNs showed bias to caudal for intracortical inputs from the upper layers. ***A***, ***B***, The integration of excitatory (***A***) and inhibitory (***B***) intralaminar inputs from rostral (−500 to 0 µm) to caudal (0–500 µm) onto CTGF (blue) and Drd1 neurons (red). The open circle represents the midpoint of the intralaminar inputs at (***i***) P7–P8 (darker color line), (***ii***) P14–P20 (darker color dotted line), and (***iii***) P60–P80 (lighter color dotted line). The black-filled circle represents the location of the recorded neurons (0,0). For developmental comparison, the lines for CTGF (blue, top) and Drd1 neurons (red, bottom) were superimposed and shown in the box at the right. The shaded areas account for 80% of responses integrated into the circuit along the rostrocaudal axis.

2000; Hanganu et al., 2002; Hoerder-Suabedissen and Molnár, 2012). Therefore, we investigated if the molecularly defined SpNs share distinct neuronal morphology. All the recorded neurons were within 100 µm from the white matter border in the ACtx. Among all the recorded neurons, 43 CTGF (P7–P9, 13; P14–P20, 16; P60–P80, 14) and 37 Drd1 neurons (P7–P9, 8; P14–P20, 13; P60–P80, 16) were reconstructed, and their distance from the white matter is plotted against age (Fig. 5*A*). Next, we categorized the reconstructed neurons into (1) pyramidal, (2) multipolar, (3) horizontal, and (4) inverted-pyramidal neurons (see details in Materials and Methods). For CTGF neurons, there were 22/42 pyramidal, 8/42 multipolar, 12/42 horizontal, and 1/42 inverted-pyramidal neurons. For Drd1 neurons, there were 22/35 pyramidal, 10/35 multipolar, 5/39 horizontal, and 0/39 inverted-pyramidal neurons. In addition, there were some pyramidal neurons with processes projecting either to the left or right from the soma, instead of projecting tangentially toward the pia (Fig. 5*B–D*). Since the number of neurons reconstructed was low, we did not statistically compare the data between genotypes or age groups. However, we did notice more angled pyramidal neurons among the pyramidal neurons class in the older age groups (# angled pyramidal neurons/total pyramidal neurons, P7–P9, CTGF = 3/7; Drd1 = 2/6; P14–P20, CTGF = 3/6; Drd1 = 3/6; P60–P80, CTGF = 8/9; Drd1 = 6/10). Next, we performed Sholl analysis to characterize dendritic morphology. At P7–P9, Sholl analysis shows that the number of intersections was similar between CTGF and Drd1 neurons (Fig. 5*E*). However, at P14–P20, there were more intersections found in the CTGF neurons compared with Drd1 neurons, particularly in the range of 100–400 µm from the soma ($p < 0.05$; rank-sum test; Fig. 5*E*). Additionally, the complexity of CTGF neurons' processes was higher than Drd1 neurons ($p = 0.04$; Kruskal–Wallis with post hoc Bonferroni's; Fig. 5*F*). Although the increase in the dendritic branching in CTGF neurons from P7–P9 to P14–P20 coincides with the developmental increment of the amount of inhibitory synaptic connections observed in CTGF SpNs (Fig. 3*D*,*E*), we did not observe any functional differences between CTGF and Drd1 neurons at P14–P20. Therefore, the complexity of SpNs' morphology does not necessarily reflect functional synapses and may not be relevant to their functional properties. Later, at P60–P80, such differences were not present, likely due to the pruning of dendrites during development regardless of cell types. Together, these results demonstrate that a diverse neuronal morphology exists even among the same molecularly defined SpNs. In addition, although CTGF and Drd1 neurons initially exhibit distinct complexity of dendritic processes, the dendrites eventually prune with age and become less distinct.

Circuit diversity in both groups of SpNs increases with age

Our functional maps and the analysis of neuronal morphology indicated a variation of intracortical inputs even within the same molecular class of SpNs (Fig. 4). In L2/3 cells, the functional diversity is lowest in the critical period and increases with further development (Meng et al., 2020). To test whether such a change in circuit diversity also occurs in SpNs, we quantified the functional circuit diversity in each group by calculating the pairwise correlation of the probability connection map (Meng et al., 2020) within each subtype and their respective age groups. If all the connectivity maps for the recorded SpNs are similar

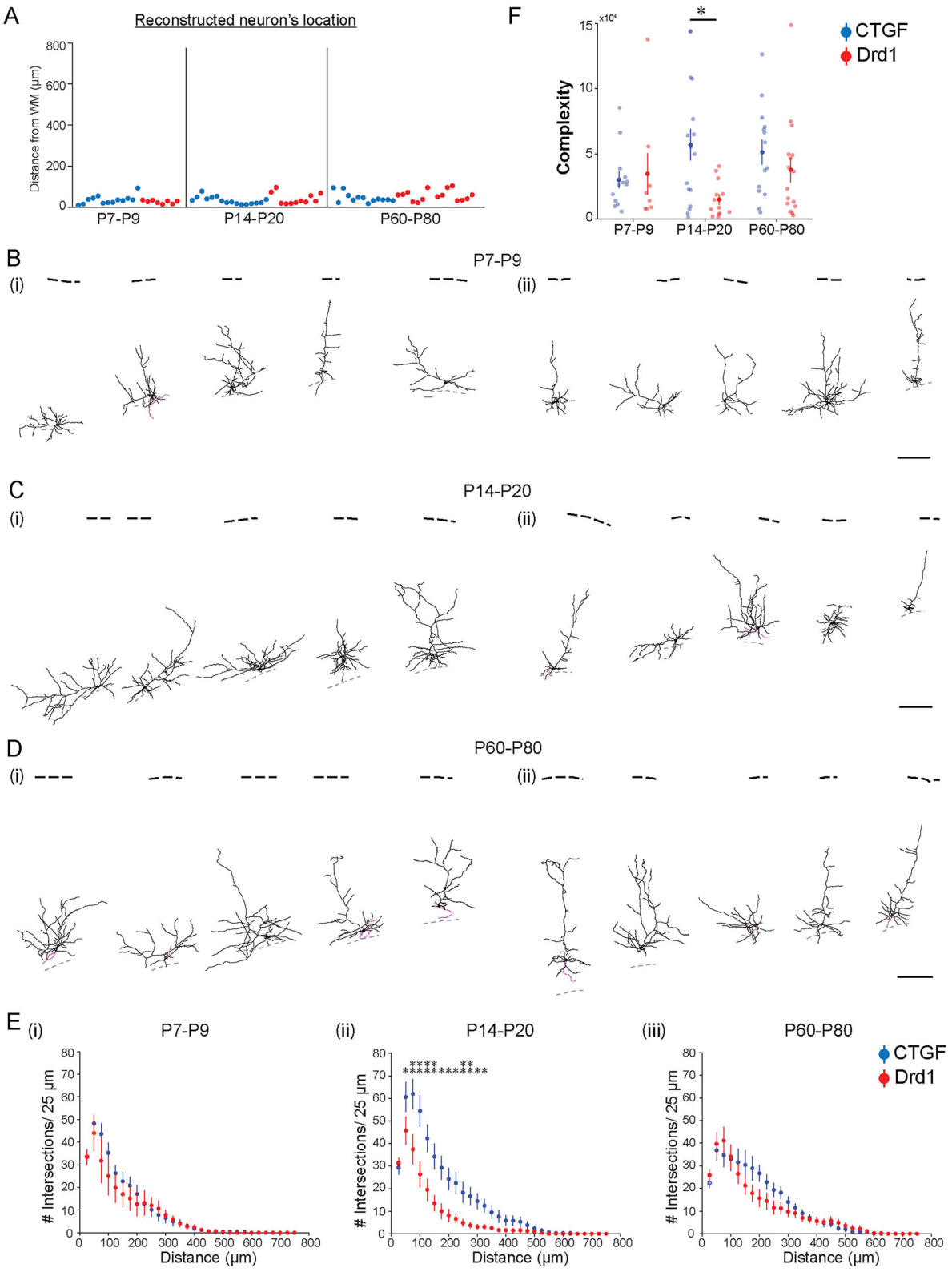


Figure 5. Neuronal morphology of CTGF and Drd1 neurons. ***A***, The location of recorded CTGF (blue) and Drd1 (red) neurons that were reconstructed with biocytin staining for different age groups. P7–P9, CTGF = 13 cells; Drd1 = 8 cells. P14–P60, CTGF = 16 cells; Drd1 = 11 cells. P60–P80, CTGF = 13 cells; Drd1 = 14 cells. ***B–D***, Examples of recorded CTGF (***i***) and Drd1 neurons (***ii***) at P7–P9 (***B***), P14–P20 (***C***), and P60–P80 (***D***). The dashed black line indicates the pial border, while the dashed light-gray line indicates the border of the white matter. In some cases, the axon was traced and shown in magenta. Scale bar, 200 µm (bottom-right). ***E***, Scholl analysis indicating the number of intersections from the soma (0 µm) toward the pia for every 25 µm radial increment for CTGF (blue) and Drd1 neurons (red). Data are represented as mean ± SEM. ***F***, Complexity of dendritic processes between CTGF (blue) and Drd1 neurons (red). Symbol * indicates $p < 0.05$ with rank-sum test. ***E***, ***F***, P7–P9, CTGF = 13 cells; Drd1 = 8 cells. P14–P60, CTGF = 16 cells; Drd1 = 13 cells. P60–P80, CTGF = 13 cells; Drd1 = 14 cells.

within the same molecular class and age group, the correlation will be high; otherwise, the correlation will be low (Fig. 6*A*). In general, both excitatory and inhibitory connection maps showed a continuous decrease in the correlation coefficient with age, for both CTGF and Drd1 neurons ($p < 0.05$; Kruskal–Wallis with post hoc Bonferroni's; Fig. 6*A*). These results suggest that there is an increase of circuit diversity with age despite their distinct molecular classes, consistent with similar observations in L2/3 (Meng et al., 2020). However, these changes occur earlier in SpNs than in L2/3 neurons, reflecting the early maturation of SpNs. When comparing both SpN subtypes in detail, CTGF neurons show more diverse excitatory and inhibitory circuit patterns than Drd1 neurons at P7–P9 (excitatory, $p = 0.02$; inhibitory, $p = 0.001$; Kruskal–Wallis with post hoc Bonferroni's). In adults, the circuit pattern for excitatory inputs was similar between CTGF and Drd1 neurons but not for inhibitory inputs where there is more diversity within the Drd1 neurons ($p < 0.001$; Kruskal–Wallis with post hoc Bonferroni's). To gain detailed insight into how inputs from each stimulation location contributed to the developmentally emerging circuit diversity, we computed the Fano factor map (see Materials and Methods). A higher Fano factor value (red) indicates higher circuit diversity and vice versa (Fig. 6*B*,*C*). The results show that the Fano factor is highest for distal inputs in both groups. Moreover, the Fano factor maps show that the excitatory inputs from lower cortical layers are similar at P7–P9 but became more diverse with age (Fig. 6*B*). Similarly, the inhibitory inputs also indicate an increase of diversity with age for both subtypes (Fig. 6*C*). Overall, the results suggest that the functional connectivity on SpNs became more diverse with age and that these changes occur earlier in SpNs than in L2/3 neurons.

The development of cortical connections on SpNs differ between CTGF and Drd1

Similar to prior studies of all SpNs (Viswanathan et al., 2012; Meng et al., 2014), within each molecular class of SpNs, we noticed a marked heterogeneity in the spatial connection patterns. We thus sought to investigate if there were underlying types ("primitives") of connection probability patterns across groups especially with respect to integration across the tonotopic axis and across the cortical laminae. For each recorded neuron, we measured the columnar extent and fraction of cortical extent (ventricle to pia) across the cortical layers of the spatial excitatory connection maps that accounted for 80% of the responses. We then plotted the cortical extent against the columnar extent (Fig. 7*A*). Most cortical inputs across the tonotopic axis fell in the 400–1,000 μm range, but the integration fraction across the cortical extent varied widely from 10 to 100% (Fig. 7*A*). To investigate if molecularly defined SpNs can be separated into different classes, we used two-dimensional *k*–means clustering on all spatial connection patterns and calculated the Dunn index to determine the optimal number of clusters (Fig. 7*B*). We found that the recorded cells could be grouped into three classes based on their spatial excitatory inputs (Fig. 7*B*). Group 1 showed extending inputs from upper layers, while Group 2 and 3 shared similar degrees of cortical extent ratio across the cortical layers, receiving inputs mostly from the lower layers. We also note that group 2 and 3 mainly differed in their integrations across the column where Group 2 was characterized by the limited coverage of columnar inputs, while Group 3 received extending inputs across the tonotopic axis. These results are consistent with prior observations (Viswanathan et al., 2012; Meng et al., 2014). To probe whether the molecular class contributes to distinct groups in intracortical connectivity, we calculated the fraction of

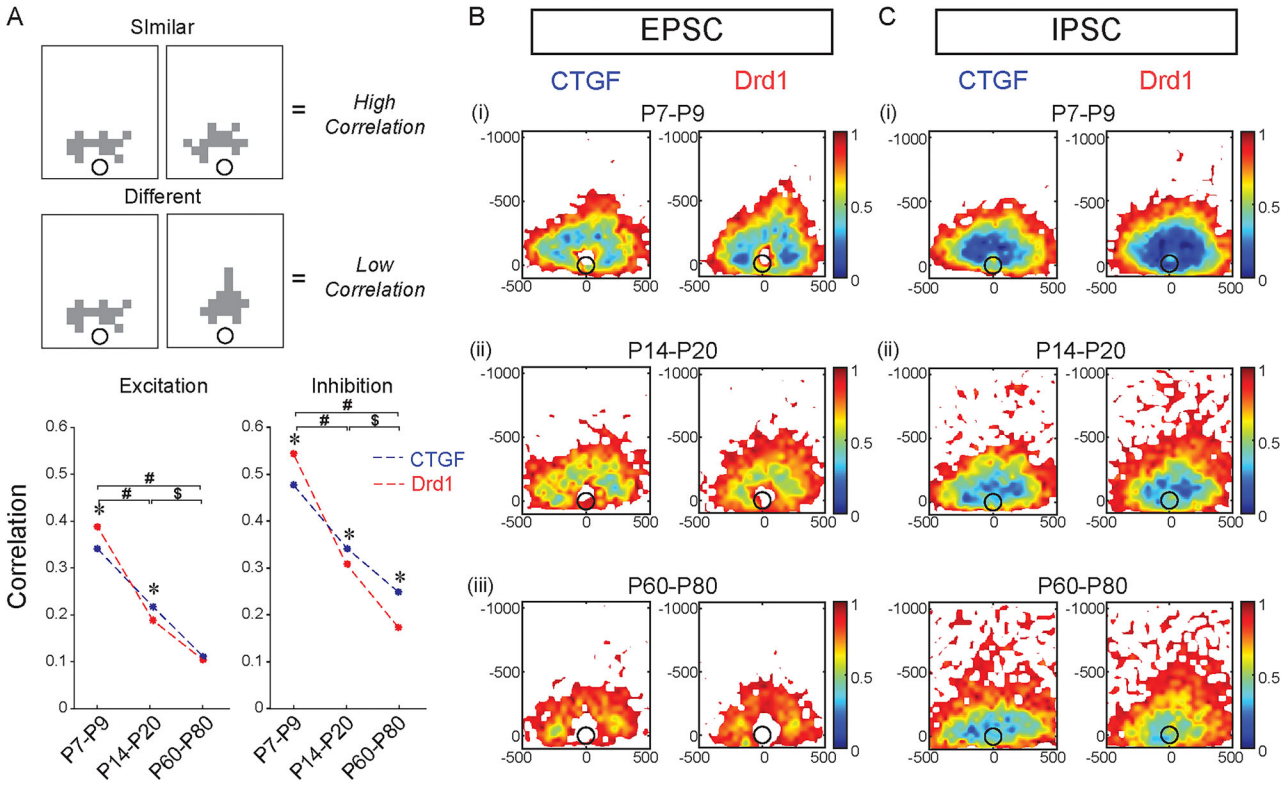


Figure 6. SpNs showed increased diversity in intracortical circuits with age. ***A***, Top, Schematic illustration of correlation of intracortical circuit maps. Higher correlation coefficient indicates similar connectivity maps within the same group and vice versa. Bottom, The correlation coefficient for excitatory and inhibitory connectivity maps for CTGF (blue) and Drd1 (red) neurons at different ages. ***B***, ***C***, The Fano factor maps for the excitatory (***B***) and inhibitory (***C***) connections for CTGF and Drd1 neurons at (***i***) P7–P9, (***ii***) P14–P20, and (***iii***) P60–P80.

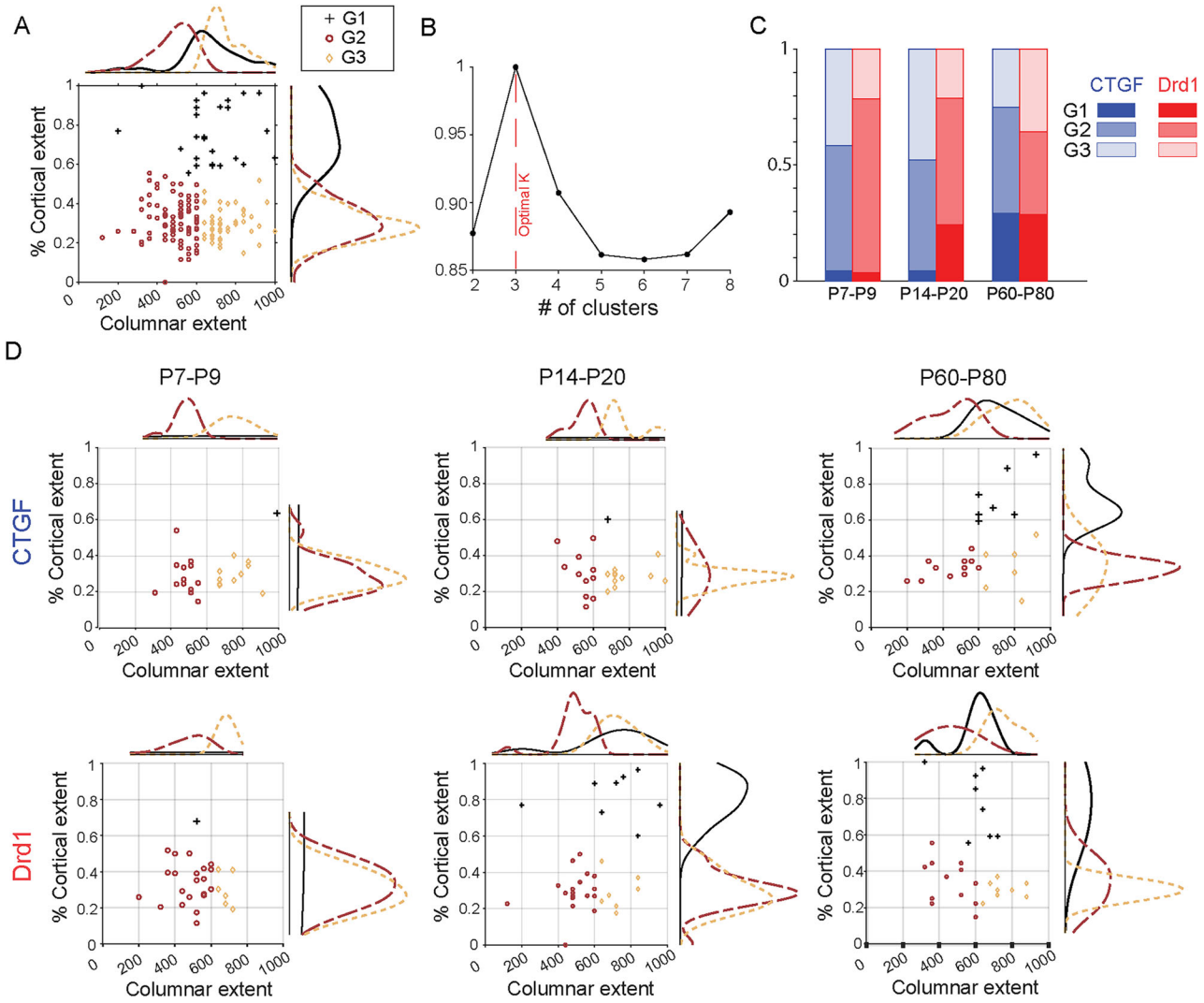


Figure 7. CTGF and Drd1 neurons form three groups based on distinct spatial input patterns. ***A***, A scatterplot of cortical extent versus columnar extent of all recorded neurons (CTGF and Drd1) mapped at −70 mV. Colors indicate the two groups based on clustering (Group1, black cross; Group 2, red open circle; Group 3, yellow diamond). Graphs on the sides indicate marginal distributions. ***B***, The optimal number of clusters (red) determined by Dunn index. ***C***, Fraction of each group in CTGF (blue) and Drd1 neurons (red) at different ages. ***D***, Scatterplots of cortical extent versus columnar extent of recorded neurons grouped based on molecule labels (top, CTGF; bottom, Drd1) and ages (left, P7–P9; middle, P14–P20; right, P60–P80). Colors indicate the two groups based on clustering (Group 1, black cross; Group 2, red open circle; Group 3, yellow diamond). Graphs on the sides indicate marginal distributions.

SpNs of each molecular type falling into each group at all age groups (Fig. 7*C*). At both time window, P7–P9 and P14–P20, most CTGF and Drd1 SpNs were dominated by Group 2 (P7–P9, CTGF = 54%; Drd1 = 75%; P14–P20, CTGF = 48%; Drd1 = 55%) followed by Group 3 (P7–P9, CTGF = 42%; Drd1 = 21%; P14–P20, CTGF = 48%; Drd1 = 21%). Meanwhile, the proportion of Group 1 was similar between CTGF and Drd1 at P7–P9 but not at P14–P20 (P7–P9, CTGF = 4%; Drd1 = 4%; P14–P20, CTGF = 4%; Drd1 = 24%). With age, the proportion of all three groups became more balanced, with a slight dominance of Group 2 (CTGF, 46%; Drd1, 36%) and the increase of Group 1 proportion in CTGF SpNs (4→29% from P14–P20 to P60–P80). To further investigate the underlying connection patterns within each cluster group, we plotted the cortical extent against the columnar extent for each molecularly labeled subgroup and age group (Fig. 7*D*). Before the ear canals opened, both subtypes of SpNs were exhibiting connection patterns that fall into Group 2 and Group 3, where cells received inputs mostly from the lower layers (Fig. 7*D*, left). At P14–P20, with the presence of more thalamocortical inputs, there were more Drd1 SpNs received intracortical inputs with higher cortical coverage (CTGF, 60%; $n = 1$; Drd1, 60–95%; $n = 8$; Fig. 7*D*, middle), suggesting that Drd1 neurons may play a more prominent role in receiving and processing thalamocortical inputs during the critical period. At P60–P80, more Group 1 neurons presented in CTGF SpNs, where their cortical extent also increased to the extent similar to Drd1 SpNs. However, there is a slight difference in their columnar inputs, where the inputs on CTGF neurons span between 600 and 1,000 μm, while those on Drd1 neurons mostly span 600–700 μm (Fig. 7*D*, right). In contrast, Group 2 and 3 SpNs showed similar levels of sparseness throughout age without any obvious indication of further small subcluster groups. These results further suggest that the development of circuits among different cell types might occur at different time points.

Discussion

SpNs are a molecularly and functionally heterogeneous neural population. Prior studies have demonstrated a diverse pattern of functional intracortical connectivity in SpNs within the ACtx during the first 2 postnatal weeks (Viswanathan et al.,

2012; Meng et al., 2014), but SpNs were recorded based on position within the subplate but without regard to the molecular subtype. As a result, there is no information on the molecular subtype and neuronal morphology of these recorded cells. Here, we aimed to use genetically labeled SpNs to explore the correlation of molecular expression, neuronal morphology, and functional intracortical circuitry. Moreover, we extended the experimental timeline to young adults (P60–P80) in the ACtx to identify if SpN properties are transformed. While the functional connectivity study on CTGF and Drd1 neurons in the somatosensory cortex has been studied (Ansorge et al., 2020; Zolnik et al., 2020, 2024; Yoneda et al., 2023), sensory cortices differ in their composition of SpN subtypes (Chang et al., 2024) and also show different maturation of their cytoarchitectural features (Chang et al., 2018). Given that the auditory system in rodents shows delineated developmental stages due to postnatal ear opening, we here focused on the ACtx.

In this study, we spatially mapped the functional synaptic inputs to molecularly defined classes of SpNs and showed that molecular subclasses of SpNs show a large amount of similarity in the excitatory synaptic connections but differ in the inhibitory synaptic connections at key developmental ages. The areas of excitatory laminar input and the respective synaptic strength for both molecular classes decrease over development, consistent with the pruning of connections. The main difference between the molecular classes is the amount of inhibitory input. The strength of inhibitory inputs in Drd1 neurons is larger at P7–P9 than in CTGF neurons, and inputs to Drd1 neurons are more extensive. Drd1 neurons also have a relatively positive shifted *E*/*I* balance index for inputs from L4, indicating the preponderance of excitatory inputs from L4 in this class of SpNs. Based on the reconstructed neuronal morphology, we observed that most Drd1 neurons have apical processes extending toward the upper layers, while CTGF neurons typically extend horizontally, parallel to the white matter (Fig. 5*C*). Since anatomical features do not necessarily correlate with function, we interpret the data cautiously. We speculate that Drd1 neurons receive more inputs from L4 than CTGF neurons at P7–P9, likely due to their morphology, which increases the likelihood of making connections with L4 neurons. Furthermore, the clustering analysis also indicated that among Drd1 neurons, there was an increase of subgroups (i.e., Group 1; Fig. 7) receiving inputs from upper layers between P14 and P20. Since Drd1 neurons project to the higher-order thalamus (Viswanathan et al., 2017; Hoerder-Suabedissen et al., 2018; Zolnik et al., 2020), we speculate that Drd1 neurons likely mediate a direct connection between thalamorecipient L4 and the higher-order thalamus. Thus, molecular classes of SpNs represent different functional circuits and likely play different roles in development.

At P14–P20, although the number of intersections found in CTGF neurons increased and was higher than in Drd1 neurons, we did not find any significant difference in the connection probability and transferred charge between the two subtypes at this age group (Figs. 2, 3). These results suggest that each dendritic branch of CTGF neurons might have fewer synapses than a dendritic branch of Drd1 neurons, suggesting differing dendritic computations in CTGF and Drd1 neurons. While ultrastructural analysis, e.g., spine analysis could be a potential measure, it is outside the scope of this study. Moreover, such a measure does not strictly correlate with functional connections, as each functional connection could involve one or multiple parallel synapses. Therefore, we did not find direct evidence suggesting a strong correlation between molecular subtypes, neuronal morphology, and functional properties.

In rodents, many SpNs survive and form L6b (Clancy et al., 2001; Hoerder-Suabedissen et al., 2018). Prior functional studies of SpN circuits focus on the first 2 postnatal weeks (Viswanathan et al., 2012; Meng et al., 2014). Our current study extends the functional understanding of SpN circuit development to adulthood and thus connects SpNs to L6b cells. Functionally, L6b neurons receive local intracortical and long-range inputs, but the different molecular classes were thought to be similar with respect to their intracortical sources in adults (Zolnik et al., 2020). Our study demonstrated that the amounts of excitatory synaptic inputs to CTGF and Drd1 neurons were similar, while inhibitory inputs from within the L6b were higher for CTGF than for Drd1 at P60–P80. The differences between studies are likely due to technical differences and/or the examined sensory area. Prior work in the somatosensory cortex used viral transfection (rabies-based monosynaptic retrograde tracing on the Drd1a-Cre and Ctgf-dgCre lines) to quantify the neurons synapsing on Drd1 and CTGF neurons (Zolnik et al., 2020); we here apply photostimulation using caged glutamate in in vitro thalamocortical slices. Our analysis is limited to the area of the thickness of the auditory thalamocortical slices, while the prior anatomical study may cover a larger volume of the somatosensory cortex. Another explanation for the differences is that the composition of CTGF and Drd1 neurons differs between somatosensory and auditory cortices (Chang et al., 2024). There are almost twofold more CTGF and Drd1 neurons in the somatosensory cortex than in the ACtx, and since the presynaptic neuron counts in the somatosensory cortex rely on the transfected starter neurons (CTGF-dgCre and Drd1-Cre), there are likely more presynapses accounted in the prior study. Moreover, our current study demonstrated differences in the functional connections of the SpN subtypes in A1. Hence, we speculate that both subtypes of SpNs might process information in a slightly different manner in each cortical area. One of the major roles of SpNs is the relay of thalamic information to L4 (Friauf and Shatz, 1991; Higashi et al., 2002; Zhao et al., 2009), and SpNs also project back to the higher-order thalamus (Viswanathan et al., 2012; Hoerder-Suabedissen et al., 2018). Sensory cortices differ in their innervation by the primary and higher-order thalamus. For example, the primary somatosensory cortex (S1) is organized in orderly barrels and septa, which differ in their thalamic innervation patterns (Feldmeyer, 2012). Similarly, A1 receives both lemniscal MGBv and nonlemniscal MGBd input, with dense MGBv inputs targeting L4 and few MGBd inputs below L4 (Vasquez-Lopez et al., 2017). We speculate that the differences in the local intracortical inputs onto SpNs between S1 and A1 are reflective of these differences.

Our results suggest that CTGF and Drd1 SpNs process information differently and may have different roles in cortical circuit processing. Such a view is consistent with observations that these two populations are differently modulated by orexin, Drd1 neurons are more sensitive to orexin than CTGF neurons, and Drd1 neurons in the primary somatosensory cortex and medial prefrontal cortex share similar functions, driving cortical oscillation (Messore et al., 2024; Zolnik et al., 2024). Such cytoarchitecture and projection patterns have also been observed in the primary visual and motor cortices (Zolnik et al., 2024); however, whether such patterns are present in the ACtx remains unclear. Given that Drd1 neurons are very sparsely distributed within the subplate of the ACtx and since their number in ACtx is significantly lower than that in the visual and somatosensory cortices (Chang et al., 2024), we speculate that in the ACtx, either a small population of Drd1 neurons would be sufficient to drive the cortical

activity as demonstrated in other cortices or another mechanism is at play.

Furthermore, sensory cortices have a different time window of the critical period in rodents (Pedrosa et al., 2022). The spine dynamics in L5 neurons differ across sensory cortices (Majewska et al., 2006), and since subplate/L6b neurons receive inputs mostly from the lower layers' neurons, we speculate that the local circuitry onto the subplate/L6b neurons differs between auditory, visual, and somatosensory cortices. During the early postnatal critical period, when connections between neurons are plastic (~P12–P18 in rodents; de Villers-Sidani et al., 2007; Barkat et al., 2011) and sensitive to environmental information, the intracortical circuit patterns of L2/3 cells are more alike but later become more diverse toward adulthood (Meng et al., 2020). SpN circuits are also sculpted by early peripheral and sensory activity in the precritcal period (<P10; Piñon et al., 2009; Meng et al., 2021; Mukherjee et al., 2022, 2023; Mukherjee and Kanold, 2023), and here, we find a similar trajectory of SpN circuitry diversity at earlier ages in SpNs than in L2/3 neurons. These results suggest that the development of circuit heterogeneity is a common process across cortical layers but occurs sequentially at different times in development. We speculate that the highest amount of circuit similarity might be a marker of the peak of the relative critical period in each layer and indicative of the potential for plasticity. Also, our analysis demonstrated that the excitatory inputs from the upper layers onto subplate/L6b neurons are biased toward the caudal direction between P7 and P9 but toward the rostral direction in the adult. Our analysis of neuronal morphology was consistent with the functional changes. Although the number of reconstructions of the recorded neurons was low, we did notice a tendency of having more pyramidal neurons with processes either projecting toward left or right, instead of tangentially toward the pial matter at P14–P20 and P60–P80 (Fig. 5). Such changes were observed after ear canals opened, and since L3/4 received thalamic inputs, we speculate that these changes are likely due to sensory experience.

SpNs could be grouped into functional subpopulations that differed in their integration across the tonotopic axis and in their columnar integration (Viswanathan et al., 2012; Meng et al., 2014), and these functional differences could be due to morphology and molecular identities. Here, while we confirm and extend this work by showing that molecular subgroups differ in the composition of functional subpopulations, we find that even within each molecular class, different types of functional circuits are present (Fig. 7). Thus, functional classes of SpNs are not defined by the expression of a single gene. Another point to note is that a previous study has demonstrated that even among Drd1 neurons, they express other SpN markers, such as CTGF and Cplx3 (Hoerder-Suabedissen et al., 2018). For example, at P8, ~34% of Drd1 neurons express CTGF marker. Therefore, we speculate that a particular signature expression profile of multiple genes would label specific functional groups. Our methods cannot address this possibility as we could not identify further if the CTGF neurons recorded were expressing Drd1 and vice versa. Additionally, given the areal differences in SpNs (Chang et al., 2024), such overlap of CTGF and Drd1 expression might differ across sensory cortices; future studies on areal sequencing would provide more conclusive ideas.

In somatosensory and visual cortices of adult rodents, L6b can be defined as a thin layer, primarily composed of multipolar excitatory neurons with axons projecting to L1/2 (Kim et al., 2024). With such definitions, the Drd1 population in somatosensory and visual cortices is not only comprised of L6b neurons, consistent with our anatomical observations (Chang et al., 2024). Although a similar tracing method would be necessary to confirm the target projections of Drd1 neurons in the ACtx, we believe that the Drd1 neurons we recorded here are more likely to be L6b rather than L6a neurons. This is because we selected neurons based on their anatomical location within the cortex (i.e., within ~100 μm from the white matter border), consistent with the location of L6b neurons ~10% from the bottom of the cortex (Kim et al., 2024). L6b neurons in the somatosensory cortex expressing CTGF and neurexophilin 4 are spiny and multipolar without apical dendrites (Kim et al., 2024). In contrast, our data showed heterogeneous neuronal morphology within CTGF and Drd1 neurons. There could be several reasons for these differences: (1) slice preparation and (2) variations between cortical areas. In our study, we used a thick auditory thalamocortical slice that preserved the rostral–caudal direction, while parasagittal sections were used to study the visual and somatosensory cortex (Kim et al., 2024). Such slice orientation may have cut off the apical dendrites projecting either rostrally or caudally. Although we aimed to obtain thicker slices (400 μm) for our recordings to preserve as many processes as possible for analysis, our method still shares some of the limitations seen in any in vitro study. Second, the definition and the maturation timing of cortical layers (Ignacio et al., 1995; Chang et al., 2018), as well as the proportion of different subtypes of SpNs (Chang et al., 2024), vary across sensory cortices. There is a possibility that these differences in neuronal morphology between ACtx and somatosensory cortex could be genetic, location, or experience dependent, with sensory cortices undergoing distinct forms of experience. To better compare neuronal morphologies across cortical areas, techniques such as brain clearing and light-sheet imaging, which preserve intact processes, would be valuable to assess whether the differences observed in various studies are due to technical differences or biological reasons. In summary, our study shows that the subplate comprises distinct molecular classes of neurons that share functional properties but differ in their associated circuits and developmental trajectories. The SpNs' molecular expression (particularly CTGF and Drd1) is not correlated to a specific neuronal morphology and functional intracortical circuitry throughout development.

References

Ansorge J, Humanes-Valera D, Pauzin FP, Schwarz MK, Krieger P (2020) Cortical layer 6 control of sensory responses in higher-order thalamus. J Physiol 598:3973–4001.

Barkat TR, Polley DB, Hensch TK (2011) A critical period for auditory thalamocortical connectivity. Nat Neurosci 14:1189–1194.

Chang M, Kanold PO (2021) Development of auditory cortex circuits. J Assoc Res Otolaryngol 22:237–259.

Chang M, Suzuki N, Kawai HD (2018) Laminar specific gene expression reveals differences in postnatal laminar maturation in mouse auditory, visual, and somatosensory cortex. J Comp Neurol 526:2257–2284.

Chang M, Nehs S, Xu Z, Kanold PO (2024) Distinct distribution of subplate neuron subtypes between the sensory cortices during the early postnatal period. J Comp Neurol 532:e25594.

Clancy B, Silva-Filho M, Friedlander MJ (2001) Structure and projections of white matter neurons in the postnatal rat visual cortex. J Comp Neurol 434:233–252.

Cruikshank SJ, Rose HJ, Metherate R (2002) Auditory thalamocortical synaptic transmission in vitro. J Neurophysiol 87:361–384.

deAzevedo LC, Hedin-Pereira C, Lent R (1997) Callosal neurons in the cingulate cortical plate and subplate of human fetuses. J Comp Neurol 386: 60–70.

de Villers-Sidani E, Chang EF, Bao S, Merzenich MM (2007) Critical period window for spectral tuning defined in the primary auditory cortex (A1) in the rat. J Neurosci 27:180–189.

Feldmeyer D (2012) Excitatory neuronal connectivity in the barrel cortex. Front Neuroanat 6:23414.
Friauf E, Shatz CJ (1991) Changing patterns of synaptic input to subplate and cortical plate during development of visual cortex. J Neurophysiol 66: 2059–2071.
Friedrichsen S, Heuer H, Christ S, Winckler M, Brauer D, Bauer K, Raivich G (2003) CTGF expression during mouse embryonic development. Cell Tissue Res 312:175–188.
Ghezzi F, et al. (2021) Non-canonical role for lpar1-egfp subplate neurons in early postnatal mouse somatosensory cortex. Elife 10:e60810.
Ghosh A, Shatz CJ (1993) A role for subplate neurons in the patterning of connections from thalamus to neocortex. Development 117:1031–1047.
Hanganu IL, Kilb W, Luhmann HJ (2002) Functional synaptic projections onto subplate neurons in neonatal rat somatosensory cortex. J Neurosci 22:7165–7176.
Higashi S, Molnár Z, Kurotani T, Toyama K (2002) Prenatal development of neural excitation in rat thalamocortical projections studied by optical recording. Neuroscience 115:1231–1246.
Hoerder-Suabedissen A, Molnár Z (2012) Morphology of mouse subplate cells with identified projection targets changes with age. J Comp Neurol 520:174–185.
Hoerder-Suabedissen A, Molnár Z (2013) Molecular diversity of early-born subplate neurons. Cereb Cortex 23:1473–1483.
Hoerder-Suabedissen A, et al. (2009) Novel markers reveal subpopulations of subplate neurons in the murine cerebral cortex. Cereb Cortex 19:1738–1750.
Hoerder-Suabedissen A, et al. (2018) Subset of cortical layer 6b neurons selectively innervates higher order thalamic nuclei in mice. Cereb Cortex 28: 1882–1897.
Ignacio M, Kimm E, Kageyama G, Yu J, Robertson R (1995) Postnatal migration of neurons and formation of laminae in rat cerebral cortex. Anat Embryol 191:89–100.
Jones EG (2000) Microcolumns in the cerebral cortex. Proc Natl Acad Sci U S A 97:5019–5021.
Kanold PO, Kara P, Reid RC, Shatz CJ (2003) Role of subplate neurons in functional maturation of visual cortical columns. Science 301:521–525.
Kanold PO, Luhmann HJ (2010) The subplate and early cortical circuits. Annu Rev Neurosci 33:23–48.
Kanold PO, Shatz CJ (2006) Subplate neurons regulate maturation of cortical inhibition and outcome of ocular dominance plasticity. Neuron 51:627–638.
Kao JPY (2006) Caged molecules: principles and practical considerations. Curr Protoc Neurosci Chapter 6:Unit 6.20.
Kim S-J, et al. (2024) A consensus definition for deep layer 6 excitatory neurons in mouse neocortex. bioRxiv:2024.11.04.621933.
Kostovic I, Rakic P (1980) Cytology and time of origin of interstitial neurons in the white matter in infant and adult human and monkey telencephalon. J Neurocytol 9:219–242.
Liao C-C, Lee L-J (2012) Evidence for structural and functional changes of subplate neurons in developing rat barrel cortex. Brain Struct Funct 217:275–292.
Luskin M, Shatz C (1985) Studies of the earliest generated cells of the cat's visual cortex: cogeneration of subplate and marginal zones. J Neurosci 5:1062–1075.
Majewska AK, Newton JR, Sur M (2006) Remodeling of synaptic structure in sensory cortical areas in vivo. J Neurosci 26:3021–3029.
Marx M, Qi G, Hanganu-Opatz IL, Kilb W, Luhmann HJ, Feldmeyer D (2017) Neocortical layer 6B as a remnant of the subplate - a morphological comparison. Cereb Cortex 27:1011–1026.
Meng X, Kao JPY, Kanold PO (2014) Differential signaling to subplate neurons by spatially specific silent synapses in developing auditory cortex. J Neurosci 34:8855–8864.
Meng X, Kao JPY, Lee HK, Kanold PO (2015) Visual deprivation causes refinement of intracortical circuits in the auditory cortex. Cell Rep 12: 955–964.
Meng X, Winkowski DE, Kao JPY, Kanold PO (2017) Sublaminar subdivision of mouse auditory cortex layer 2/3 based on functional translaminar connections. J Neurosci 37:10200–10214.
Meng X, Solarana K, Bowen Z, Liu J, Nagode DA, Sheikh A, Winkowski DE, Kao JPY, Kanold PO (2020) Transient subgranular hyperconnectivity to L2/3 and enhanced pairwise correlations during the critical period in the mouse auditory cortex. Cereb Cortex 30:1914–1930.
Meng X, Mukherjee D, Kao JPY, Kanold PO (2021) Early peripheral activity alters nascent subplate circuits in the auditory cortex. Sci Adv 7:9155–9167.
Messore F, et al. (2024) An orexin-sensitive subpopulation of layer 6 neurons regulates cortical excitability and anxiety behaviour. bioRxiv:2024.07.25.605138.
Molnár Z, Luhmann HJ, Kanold PO (2020) Transient cortical circuits match spontaneous and sensory-driven activity during development. Science 370:eabb2153.
Mukherjee D, Kanold PO (2023) Changing subplate circuits: early activity dependent circuit plasticity. Front Cell Neurosci 16:1067365.
Mukherjee D, Meng X, Kao JPY, Kanold PO (2022) Impaired hearing and altered subplate circuits during the first and second postnatal weeks of otoferlin-deficient mice. Cereb Cortex 32:2816–2830.
Mukherjee D, Xue B, Chen CT, Chang M, Kao JPY, Kanold PO (2023) Early retinal deprivation crossmodally alters nascent subplate circuits and activity in the auditory cortex during the precritical period. Cereb Cortex 33: 9038–9053.
Muralidharan S, Dirda NDA, Katz EJ, Tang CM, Bandyopadhyay S, Kanold PO, Kao JPY (2016) Ncm, a photolabile group for preparation of caged molecules: synthesis and biological application. PLoS One 11:e0163937.
Oswald AMM, Reyes AD (2008) Maturation of intrinsic and synaptic properties of layer 2/3 pyramidal neurons in mouse auditory cortex. J Neurophysiol 99:2998–3008.
Oswald AMM, Reyes AD (2011) Development of inhibitory timescales in auditory cortex. Cereb Cortex 21:1351–1361.
Pedrosa LRR, Coimbra GDS, Corrêa MG, Dias IA, Bahia CP (2022) Time window of the critical period for neuroplasticity in S1, V1, and A1 sensory areas of small rodents: a systematic review. Front Neuroanat 16:763245.
Pillai AG, de Jong D, Kanatsou S, Krugers H, Knapman A, Heinzmann JM, Holsboer F, Landgraf R, Joëls M, Touma C (2012) Dendritic morphology of hippocampal and amygdalar neurons in adolescent mice is resilient to genetic differences in stress reactivity. PLoS One 7:38971.
Piñon MC, Jethwa A, Jacobs E, Campagnoni A, Molnár Z (2009) Dynamic integration of subplate neurons into the cortical barrel field circuitry during postnatal development in the Golli-tau-eGFP (GTE) mouse. J Physiol 587:1903–1915.
Price DJ, Aslam S, Tasker L, Gillies K (1997) Fates of the earliest generated cells in the developing murine neocortex. J Comp Neurol 377:414–422.
Robertson RT, Annis CM, Baratta J, Haraldson S, Ingeman J, Kageyama GH, Kimm E, Yu J (2000) Do subplate neurons comprise a transient population of cells in developing neocortex of rats? J Comp Neurol 426:632–650.
Rockland KS (2010) Five points on columns. Front Neuroanat 4:22.
Sheikh A, Meng X, Liu J, Mikhailova A, Kao JPY, McQuillen PS, Kanold PO (2019) Neonatal hypoxia–ischemia causes functional circuit changes in subplate neurons. Cereb Cortex 29:765–776.
Shepherd GMG, Pologruto TA, Svoboda K (2003) Circuit analysis of experience-dependent plasticity in the developing rat barrel cortex. Neuron 38:277–289.
Suter BA, O'Connor T, Iyer V, Petreanu LT, Hooks BM, Kiritani T, Svoboda K, Shepherd GMG (2010) Ephus: multipurpose data acquisition software for neuroscience experiments. Front Neural Circuits 4:1789.
Takesian AE, Bogart LJ, Lichtman JW, Hensch TK (2018) Inhibitory circuit gating of auditory critical period plasticity. Nat Neurosci 21:218.
Tolner EA, Sheikh A, Yukin AY, Kaila K, Kanold PO (2012) Subplate neurons promote spindle bursts and thalamocortical patterning in the neonatal rat somatosensory cortex. J Neurosci 32:692–702.
Valverde F, Facal-Valverde MV (1988) Postnatal development of interstitial (subplate) cells in the white matter of the temporal cortex of kittens: a correlated Golgi and electron microscopic study. J Comp Neurol 269:168–192.
Valverde F, Facal-Valverde MV, Santacana M, Heredia M (1989) Development and differentiation of early generated cells of sublayer VIb in the somatosensory cortex of the rat: a correlated Golgi and autoradiographic study. J Comp Neurol 290:118–140.
Valverde F, Lopez-Mascaraque L, Santacana M, De Carlos J (1995) Persistence of early-generated neurons in the rodent subplate: assessment of cell death in neocortex during the early postnatal period. J Neurosci 15: 5014–5024.
Vasquez-Lopez SA, Weissenberger Y, Lohse M, Keating P, King AJ, Dahmen JC (2017) Thalamic input to auditory cortex is locally heterogeneous but globally tonotopic. Elife 6:e25141.
Viswanathan S, Bandyopadhyay S, Kao JPY, Kanold PO (2012) Changing microcircuits in the subplate of the developing cortex. J Neurosci 32: 1589–1601.
Viswanathan S, Sheikh A, Looger LL, Kanold PO (2017) Molecularly defined subplate neurons project both to thalamocortical recipient layers and thalamus. Cereb Cortex 27:4759–4768.

Wahle P, Meyer G, Wu JY, Albus K (1987) Morphology and axon terminal pattern of glutamate decarboxylase-immunoreactive cell types in the white matter of the cat occipital cortex during early postnatal development. Dev Brain Res 36:53–61.

Wess JM, Isaiah A, Watkins PV, Kanold PO (2017) Subplate neurons are the first cortical neurons to respond to sensory stimuli. Proc Natl Acad Sci U S A 114:12602–12607.

Xue B, Meng X, Kao JPY, Kanold PO (2023) Age-related changes in excitatory and inhibitory intra-cortical circuits in auditory cortex of C57Bl/6 mice. Hear Res 429:108685.

Yoneda T, Hayashi K, Yoshimura Y (2023) Experience-dependent functional plasticity and visual response selectivity of surviving subplate neurons in the mouse visual cortex. Proc Natl Acad Sci U S A 120:e2217011120.

Yu I-S, Chang H-C, Chen K-C, Lu Y-L, Shy H-T, Chen C-Y, Lee K-Y, Lee L-J (2019) Genetic elimination of connective tissue growth factor in the forebrain affects subplate neurons in the cortex and oligodendrocytes in the underlying white matter. Front Neuroanat 13:16.

Zhao C, Kao JPY, Kanold PO (2009) Functional excitatory microcircuits in neonatal cortex connect thalamus and layer 4. J Neurosci 29:15479–15488.

Zolnik TA, Ledderose J, Toumazou M, Trimbuch T, Oram T, Rosenmund C, Eickholt BJ, Sachdev RNS, Larkum ME (2020) Layer 6b is driven by intracortical long-range projection neurons. Cell Rep 30:3492–3505.e5.

Zolnik TA, Bronec A, Ross A, Staab M, Sachdev RNS, Molnár Z, Eickholt BJ, Larkum ME (2024) Layer 6b controls brain state via apical dendrites and the higher-order thalamocortical system. Neuron 112:805–820.e4.